Wiley Online Library
Early View publication on www.wileyonlinelibrary.com
(issue and page numbers not yet assigned;
citable using Digital Object Identifier – DOI)

Phys. Status Solidi A, 1700293 (2017) / DOI 10.1002/pssa.201700293

physica status solidi a
www.pss-a.com
applications and materials science

Review Article

Dielectric surface passivation for silicon solar cells: A review

Ruy S. Bonilla*[,1], Bram Hoex[2], Phillip Hamer[1,2], and Peter R. Wilshaw[1]

[1] Department of Materials, University of Oxford, Parks Rd, Oxford OX1 4NH, United Kingdom
[2] School of Photovoltaic and Renewable Energy Engineering, The University of New South Wales, Sydney, NSW 2052, Australia

Received 1 March 2017, revised 10 May 2017, accepted 10 May 2017
Published online 14 June 2017

Keywords chemical vapour deposition, dielectric coatings, silicon solar cells, surface passivation

* Corresponding author: e-mail sebastian.bonilla@materials.ox.ac.uk, Phone: +44 18652 83097, Fax: +44 (0)1865 273789

Silicon wafer solar cells continue to be the leading photovoltaic technology, and in many places are now providing a substantial portion of electricity generation. Further adoption of this technology will require processing that minimises losses in device performance. A fundamental mechanism for efficiency loss is the recombination of photo-generated charge carriers at the unavoidable cell surfaces. Dielectric coatings have been shown to largely prevent these losses through a combination of different passivation mechanisms. This review aims to provide an overview of the dielectric passivation coatings developed in the past two decades using a standardised methodology to characterise the metrics of surface recombination across all techniques and materials. The efficacy of a large set of materials and methods has been evaluated using such metrics and a discussion on the current state and prospects for further surface passivation improvements is provided.

1 Introduction Silicon wafer solar cells are the fastest growing and most successful photovoltaic technology to date. The past decade witnessed remarkable technical and economical milestones: (i) record breaking single junction cells with power conversion efficiencies exceeding 26% [1]; (ii) multicrystalline silicon cells, which account for over 60% of the PV market, that now have efficiencies exceeding 20% [2]; (iii) a continued average annual growth in the PV market of more than 40% over the past decade [3]; (iv) a vast reduction in module production costs bringing the $\$/W_p$ of solar energy below grid parity in many places around the world; and (v) energy payback times now below 1 year [4, 5].

To keep the growth and deployment of this technology, industry and academics continue to research ways to increase cell efficiency and/or reduce its production cost. Out of these two approaches, improved efficiency has the greatest scope to impact the overall cost of solar electricity since it affects the entire value chain [6–8]. The production and processing of silicon has largely improved in the past decades. This has reduced the negative effects of bulk impurities in cell performance. Cost reduction has also driven cells to become increasingly thinner. These successes meant that the efforts to improve further device performance have shifted towards surface physical phenomena, mainly the passivation of surfaces and interfaces. Surface passivation helps to prevent unwanted recombination of photogenerated electron–hole pairs. As such, it is a key requirement to achieve high conversion efficiencies. In fact, a large portion of the improvement achieved in record-breaking silicon cells has been possible due to outstanding surface passivation. This is demonstrated, for example, by the use of amorphous silicon passivation in Kaneka's 26.6% [9] and Panasonic's 25.6% [10] cells, or aluminium oxide passivation of p-type silicon combined with thin oxide electron selective contacts in Fraunhofer ISE 25.7% TOPCon cell [11].

The surfaces in a solar cell form an abrupt discontinuity to the semiconductor crystal lattice. This means that the band structure of the material is disrupted and a semi-continuum of energy states arise in the previously forbidden bandgap. These states correspond to strained or unterminated, also referred to as dangling, surface bonds. Recombination mediated by bandgap states is best described using the well-known Shockley–Read–Hall [12, 13] theory, extended to a continuum of surface states [14–16]. In the case of the semiconductor surface, a good estimation can be achieved

by approximating the recombination activity of interface states of all energies, into a concentration D_{it} of states at a single energy in the middle of the gap ($E_t - E_i = 0$). The states at this energy have electron recombination velocity $S_{n0} = v_{th} D_{it} \sigma_n$, and hole capture velocity $S_{p0} = v_{th} D_{it} \sigma_p$, where σ indicates the capture cross section of the states. The total recombination at the surface is then characterised by the effective surface recombination velocity (SRV) as follows:

$$S_{eff} = \frac{U_s}{\Delta n(x=d)} = \frac{1}{\Delta n_d} \frac{n_s p_s - n_i^2}{(n_s + n_i)/S_{p0} + (p_s + n_i)/S_{n0}}. \quad (1)$$

where n_s, p_s represent the steady-state carrier concentrations at the surface, Δn_d represents the excess minority carrier concentration at the edge of the space charge region (of width d) formed at the surface of the semiconductor due to surface charge [17], and n_i represents the intrinsic carrier concentration. The lower the effective SRV the better the surface is from the point of view of device performance since fewer carriers are lost in recombination processes.

An examination of Eq. (1) shows that there are two complementary ways of reducing surface recombination. First by reducing the rate by which interface states capture electrons and holes, either by having fewer states or lower capture probabilities, represented together by the S_{n0}, S_{p0} parameters. This is achieved by completing the dangling bonds using a surface dielectric coating or chemical species – usually hydrogen, and is commonly referred to as the chemical component of passivation. Second, since a recombination process requires the presence of both electrons and holes, lower recombination rates are achieved by reducing the number of one type of carriers available at the surface, n_s or p_s, by changing their ratio at the surface p_s/n_s, which is constant for steady-state conditions. The minority carrier at the surface normally determines the rate of recombination. This is often but not necessarily the bulk minority carrier and thus in n-type Si, a lower hole to electron ratio (p_s/n_s) would reduce surface recombination. This reduction can be achieved in two distinct ways. The first is achieved by an electric field that penetrates the semiconductor surface and thus modifies the surface carrier concentration. This is referred to as the field-effect component of surface passivation. The electric field is often established by a fixed charge density Q_f in the dielectric film which creates a mirror charge in the surface region of the silicon. The second strategy is the in-diffusion of a high concentration of dopants of either carrier type near the surface. This produces an equilibrium near-surface charge carrier gradient, which in the case of compensating dopants is also known as an emitter. When such an emitter does not fulfill a carrier collection task it is termed a floating emitter. This manuscript predominantly focusses on dielectric chemical and field-effect passivation, and presents a review of the surface dielectrics developed in the past two decades. The field-effect passivation (FEP) coming from diffused emitters is not within the scope of this review, yet it will be noted when it is used in combination with dielectric coating passivation.

An observation is made with regards to nomenclature. Here, the widely adopted field-effect passivation terminology has been used, but it is important to note that, in the absence of external stimulation, the electric field and associated charge distribution established in the near surface region is in equilibrium. Therefore the electric field cannot repel excess minority carriers away from the surface. This electric field, however, modifies the surface carrier concentration, which in regimes of heavy accumulation and inversion, leads to a reduction in recombination rates upon carrier excitation. Thus, strictly speaking, the reduction in surface recombination is due to the spatial change in carrier concentration near the surface, which in turn is due to the electric field. This distinction has recently been pointed out by Cuevas [18, 19]. However, the term 'field-effect passivation' has been retained for the present work since it is in wide use throughout the literature and it is clear that an electric field is created in the silicon near surface region by doping or by dielectric charge, as originally pointed in the early 1950s by Shockley and Pearson [20, 21] in the context of the field-effect transistor.

Girisch et al. [15] and Aberle et al. [16] proposed a solution algorithm for Eq. (1) that included the contribution from photo-generated carriers and accounted for dielectric film charge Q_f, the silicon surface space charge region $Q_{Si}(n_s, p_s)$, and charged interface states Q_{it}. Figure 1 illustrates the solution to Eq. (1) using this algorithm for a typical Si–SiO_2 interface. Here the chemical and field-effect aspects of surface passivation can be distinguished. The

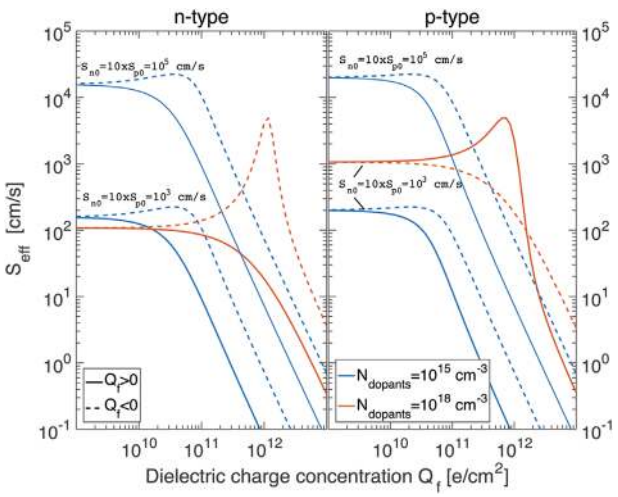

Figure 1 Effective SRV as a function of positive and negative dielectric charge concentration Q_f for, n and p-type silicon with $S_{n0} = 10 \times S_{p0}$, $\Delta n_d = 10^{15}\,cm^{-3}$, dopant concentration $N_{dopants}$, and uniform interface charge $Q_{it} = 10^{11}\,e/cm^{-2}$.

effect of slower capture rates is simply to lower the overall SRV as evident in the bottom solid blue trace. The effect of dielectric charge concentration is examined in more detail for n- and p-type silicon of different doping levels. First, it is noted that positive charge (solid trace) normally provides better passivation than negative charge (dashed trace). This is due to the higher capture velocity of electrons, compared to that of holes which is commonly observed at dielectric–silicon interfaces, particularly for the Si–SiO_2 interface where the ratio is found to be ~10–100 [16]. Secondly, S_{eff} scales with the surface dopant density when FEP is the dominant passivation mechanism. This was shown by McIntosh and Black in Ref. [22]. Previously, this increase had been incorrectly attributed to a larger carrier recombination rate (S_{n0}, S_{p0}) at highly doped surfaces. It is actually found that the fundamental recombination rate at, e.g. Si-Al_2O_3 surfaces, is independent of the surface dopant density [22, 23].

When a dielectric film is used to passivate the silicon surface it is possible, and likely, that both chemical and field-effect passivation are present. Distinguishing between these can elucidate ways in which more *effective* passivation is achieved. In this review, whenever possible, the data reported in the literature will be used to infer the influence of each of these mechanisms.

2 Characterising surface passivation

A number of metrics have been used to characterise the amount of recombination taking place at a semiconductor surface. To produce a comparative review of different passivation dielectrics, the metrics and experimental methodologies commonly used to infer them will be reviewed in this section.

2.1 Surface recombination velocity

The SRV was the first quantity experimentally measured since it related directly to the SRH description of defect-mediated recombination at the surface, as described in Section 1. Initial measurements of SRV were deduced from current density measurements in *pn* junction diodes either with a gate-controlled bias [14, 24], or photo-generation of carriers far from the junction using a bias light [15, 25–27]. At present, contactless photoconductance (PC) decay or transient measurements [28] of effective lifetime (τ_{eff}), from which SRV can be extracted, is the preferred technique since it does not require a device structure or direct contacts, and can examine larger areas. In PC measurements the conductance, and thus the change in minority carrier concentration, is measured using either microwaves [29–31] or inductive coupling [32–36]. Out of these two, inductive coupling PC has become the technique of choice for minority carrier lifetime measurements in silicon, largely due to the developments by Ron Sinton [37, 38] via his company Sinton Instruments [39] in the past decades.

Measurements of effective lifetime contain the contributions of all recombination mechanisms in the bulk and at the surface of the specimens:

$$\frac{1}{\tau_{eff}} = \frac{1}{\tau_b} + \frac{1}{\tau_s}. \tag{2}$$

Increasing both these lifetimes is key to improving cell performance. The bulk component τ_b includes the intrinsic components due to Auger and radiative recombination [40], which will here be described by Richter's parameterisation [41], with the radiative recombination term B_{rel} from Ref. [42] and B_{low} from Ref. [43]. It also includes defect-mediated SRH recombination mainly arising from bulk impurities. Surface passivation studies are normally conducted in high quality Float Zone (FZ) silicon, where SRH bulk lifetime is sufficiently high that the bulk recombination is negligible relative to other recombination mechanisms. Grant et al. [44–46] have recently showed that grown-in bulk defects can be activated in FZ-Si when annealed, resulting in substantial recombination. They also demonstrated the conditions required to minimise their effect. These defects and their energy states, however, have not yet been fully studied. In this paper, to account for bulk recombination and so find τ_s, an injection-independent bulk SRH lifetime τ_{SRH} is used in an iterative algorithm as proposed by Kimmerle et al. [47]:

$$\frac{1}{\tau_s} = \frac{1}{\tau_{eff}} - \frac{1}{\tau_{Rad}} - \frac{1}{\tau_{Aug}} - \frac{1}{\tau_{SRH}}. \tag{3}$$

The algorithm is described in Section 2.2 where it is used to determine J_{0s}. For the calculation of SRV, the SRH bulk lifetime is assumed infinite to minimise the propagation of error in the calculation.

The surface lifetime component τ_s has a complex dependence on SRV. The amount of recombination at the surface depends on the spatial variation of the injected carriers. Carriers generated far from the surface may only recombine when they diffuse to the surface. Similarly, carriers generated at the surface may recombine instantaneously or diffuse to the bulk. To account for this dependence, Luke and Cheng [48] developed a formalism and found a solution that indicates that the effective SRV is a function of an infinite sum of decaying exponential terms of effective lifetime, where the first mode is dominant and is written as follows:

$$S_{eff} = \sqrt{D\left(\frac{1}{\tau_s}\right)}\tan\left(\frac{W}{2}\sqrt{\frac{1}{D}\left(\frac{1}{\tau_s}\right)}\right), \tag{4}$$

where W is the specimen width and D is the ambipolar carrier diffusion coefficient. For sufficiently low SRV, $\tan(x) \approx x$, and the SRV can be approximated to

$$S_{eff} = \left(\frac{1}{\tau_{eff}} - \frac{1}{\tau_B}\right)\frac{W}{2} \tag{5}$$

This expression has been widely used to characterise SRV, as its accuracy is better than 4% when recombination is the same at both surfaces and $(S_{\text{eff}}W)/D < 1/4$ [49]. Since some of the specimens, for example textured silicon, may not fulfill this requirement, the effective SRV in all works referenced in this review is calculated from the reported PC measurements of τ_{eff} using Eq. (4), and D as a function of Δn using Klaassen's mobility model [50] as implemented in PV Lighthouse [51].

From Eq. (5) it is also clear that for a given level of surface passivation, the effective lifetime increases for thicker samples, and higher bulk intrinsic lifetimes, corresponding to a lower doping. S_{eff} is therefore the preferred metric to assess the passivation quality of a dielectric film. An important distinction to draw, however, is that the *effective* SRV, as used here, relates to the recombination current at a virtual surface at the edge of the space charge region, rather than the recombination occurring at the actual surface. This is because calculating and measuring the excess carrier concentration Δn at the actual surface is a rather involved task. This definition of S_{eff} has been widely accepted [17].

2.2 Surface saturation current The second metric used to characterise surface recombination is the emitter saturation current density J_{0e}. This quantity has been more generally used to assess the combined recombination from surface states and a highly doped emitter. It has become very popular as it can be used to evaluate the quality of an emitter, from the point of view of recombination, using measurements of τ_{eff} and Kane and Swanson's well-known method [35]. Recently, McIntosh and Black [22] proposed the surface saturation current density J_{0s} metric, which relates directly to J_{0e} when SRH and Auger recombination in the emitter are negligible, and showed that it provides a better comparison of dielectric passivation quality in specimens without an emitter (undiffused) when field-effect passivation is significant. They demonstrated that in such undiffused specimens J_{0s} is independent of the surface dopant concentration under most practical conditions, and it is thus a superior metric of passivation quality in dielectric films.

J_{0s} values reported in this review have been determined from the values presented in the original manuscripts by following a similar iterative procedure as suggested by Kimmerle et al. [47], which was developed from the work of Mäckel and Verner [52]. First, τ_{SRH} is assumed infinite and J_0 is calculated from a PC measurement of τ_{eff} as follows:

$$J_0(\Delta n) = \frac{d}{d\Delta n}\left(n_{\text{i,eff}}^2 \cdot \sqrt{D\left(\frac{1}{\tau_s}\right)}\tan\left(\frac{W}{2}\sqrt{\frac{1}{D}\left(\frac{1}{\tau_s}\right)}\right)\right), \tag{6}$$

where Auger and radiative recombination are again described by Richter's parameterisation [41], and the effective intrinsic concentration $n_{\text{i,eff}}(\Delta n)$ is calculated using the online PV Lighthouse [51] implementation of Pässler's model [53]. Following on Mäckel and Verner's suggestions, the J_{0s} value has been calculated as the average around the ±10% of the flattest part of the $J_0(\Delta n)$ curve. The flattest part was defined by the minimum of $dJ_0(\Delta n)/d\Delta n$. After finding an injection-independent J_{0s}, the SRH term that satisfies

$$\frac{J_{0s} * (N_{\text{dop}} + \Delta n)}{q n_{\text{i,eff}}^2} = \sqrt{D\left(\frac{1}{\tau_s}\right)}\tan\left(\frac{W}{2}\sqrt{\frac{1}{D}\left(\frac{1}{\tau_s}\right)}\right), \tag{7}$$

and is found numerically using a Nonlinear Least Squares minimisation in Matlab. Once a $\tau_{\text{SRH}}(\Delta n)$ is found, an average injection-independent τ_{SRH} is found averaging the same range of Δn as previously done for $J_0(\Delta n)$. This procedure is iterated until τ_{SRH} and J_{0s} change marginally. The resultant value of τ_{SRH} is then used in τ_s to find S_{eff}.

An important insight to draw from Mäckel and Verner's study is the large variation that can exist in the determination of J_{0s} depending on the sample and measuring technique. To counteract this, the surface recombination metrics reported here will concentrate on studies using semi-uniform illumination, by using the IR-filtered flash lamp in the standard WCT Sinton system, a base dopant resistivity as close to 1 Ωcm as possible, and no emitter such that, in absence of band bending, the surface carrier concentration is the same as in the bulk. Additionally, the same intrinsic bulk recombination models are applied to all effective lifetime measurements, and the extraction of J_{0s} is kept within the $0.5 \times N_{\text{dop}} < \Delta n < 5 \times N_{\text{dop}}$ range.

2.3 Implied open-circuit voltage The implied open-circuit voltage, abbreviated iV_{oc}, is the third metric that will be used here to compare the quality of different dielectrics and deposition techniques at passivating the silicon surface. This can be calculated from the known Δn values obtained from a measurement of $\tau_{\text{eff}}(\Delta n)$ using PCD. As detailed by Cuevas and Sinton [54], iV_{oc} is given by

$$iV_{\text{oc}} = \frac{kT}{q}\ln\left(\frac{\Delta n(N_{\text{dop}} + \Delta n)}{n_{\text{i,eff}}^2}\right) \tag{8}$$

Unfortunately, the generation data required to calculate the equivalent suns intensity for a Δn in a given sample is not widely available in the literature and thus, the iV_{oc} calculated here is obtained as a function of Δn rather than Suns. Unless otherwise indicated all values of τ_{eff}, S_{eff} and iV_{oc} will be reported at a minority carrier injection of $\Delta n = 10^{15}\,\text{cm}^{-3}$.

2.4 Textured surfaces The effect of texturing the silicon surface is also considered in this work. Texturing of the solar cell's surface is an integral part of the manufacturing process as it enhances photon capture and trapping. A large number of methods to texture silicon have

been developed, however, the random upright pyramids formed using a buffered alkaline etchant (typically buffered KOH) is the commercially standard method in monocrystalline silicon [55]. Despite the fact that all practical solar cells only exhibit textured surfaces, at least on the front surface, much less data have been reported for recombination parameters for textured specimens than for flat ones. These data are presented here but the following considerations must be noted with regards to surface recombination metrics for textured silicon.

Recombination at a textured surface is generally larger than for a flat surface of an equivalent specimen. This is firstly due to the increase in surface area when the texturing is formed. The texturing processes for single crystal silicon typically produce a random pyramidal morphology with an area about 73% larger [17, 55] than the pre-existing {100} surfaces commonly used. The faces of the pyramids are approximately {111} surfaces and McIntosh and Johnson [55] demonstrated that the increase in recombination on textured material was not only associated with the extra surface area, but also due to the larger number of dangling bonds at a {111} surface, and also the higher concentration of interface defects in a textured surface, possibly originating from mechanical stress in the dielectric–silicon interface at creases, edges or vertices. Baker-Finch and McIntosh [56] characterised the contributions of the latter.

These differences have been commonly taken into account by simply multiplying J_{0s} by a scaling factor such that flat and textured surfaces are assumed comparable [55, 57, 58]. However, as shown by McIntosh and Johnson [55], the value of such a factor depends strongly on the texturing process and the surface dopant concentration. For this reason, the metrics reported for textured silicon in this review are calculated in the same way as for flat silicon samples *without* a scaling factor, and should only be compared to similarly textured specimens.

3 The impact of surface passivation on cell performance

The requirement of higher efficiency solar cells is currently driving industry into adopting better performing architectures [2]. The passivated emitter rear cell (PERC) and the interdigitated back contacted (IBC) cell are among the most promising designs for high efficiency in the coming decades [59]. To provide an indication of how dielectric surface passivation affects the performance of devices, a number of simulations have been conducted here using EDNA 2 [60] and Quokka 2.2.4 [61]. In Quokka, surface recombination is better modelled by the J_{0e} parameter when moderate or large charge concentrations are present in the dielectric, or when the surface has the added field-effect from an emitter or surface field. The J_{0e} parameter for the front surface of the cells modelled here varied between 1 and 1000 fA cm^{-2}. This simulates a wide range of surface recombination at the front of the cell.

A typical PERC p-type cell with a local aluminium back surface field (BSF) and screen-printed metallisation has been chosen, as reported by Fell in 2014 [62]. Two different front emitters were modelled to evaluate the effect of the industry trend towards lighter doping. The parameters for the modelled PERC cell are listed in Table 1. Figure 2a illustrates a simulation of the J_{0e} parameter. This was conducted in EDNA 2 to quantify the effect that chemical and field-effect passivation have on the front surface recombination parameters J_{0e} and S_{eff}. It is noted here that a similar simulation of J_{0e} can also be done as suggested by Cabanas-Holmen and Basore [63] using a semi-ideal lightly doped *pn* junction, with negligible *p* side recombination in PC1D [64]. In Fig. 2a, it is evident that lighter-doped emitters are beneficial from the point of view of surface recombination when moderate chemical passivation is provided. Lighter-doped emitters also gain more passivation from the field-effect mechanism. As the chemical passivation worsens, the field-effect is of lesser importance. This is due to the marginal change in carrier concentration induced by the field in a surface with already very low concentration of minority (holes) carriers. Overall it can be seen that $J_{0e,front}$ can vary strongly depending on the quality of chemical passivation, and only benefits when a substantial concentration of charge is mirrored in the space charge region, as a result of the dielectric film charge. This indicates that for PERC cells the field-effect mechanism is of lesser importance than the chemical.

Figure 2b illustrates the efficiency of the simulated PERC cell when front surface recombination is varied, as represented by the J_{0e} parameter. It is clear that the performance of this cell is dependent on the passivation of both front and back surfaces. As the passivation decreases,

Table 1 Summary of cell parameters used for simulations in Quokka.

parameter	PERC	IBC
cell thickness	180 μm	180 μm
base doping	p	n
base resistivity	1 Ωcm	1 Ωcm
SRH bulk lifetime	$\tau_n = 0.5$, $\tau_p = 3$ ms	$\tau_n = \tau_p = 5$ ms
emitter diffusion ρ_{sheet}	100,150 Ω/□	90 Ω/□
base diffusion ρ_{sheet}	60 Ω/□	50 Ω/□
front surface field ρ_{sheet}	–	200 Ω/□
undiffused rear J_0, passivated	13, 130 fA cm^{-2}	2 fA cm^{-2}
emitter diffusion J_0, passivated	–	19, 200 fA cm^{-2}
emitter diffusion J_0, contacted	600 fA cm^{-2}	417 fA cm^{-2}
base diffusion J_0, passivated	–	215 fA cm^{-2}
base diffusion J_0, contacted	800 fA cm^{-2}	583 fA cm^{-2}
emitter contact resistance	2×10^{-3} Ωcm^2	5×10^{-5} Ωcm^2
base contact resistance	5×10^{-3} Ωcm^2	1×10^{-5} Ωcm^2
external series resistance	0.1 Ωcm^2	0.1 Ωcm^2
external shunt resistance	10^5 Ωcm^2	10^5 Ωcm^2
$n_{i,eff}$	9.65×10^9 cm^{-3}	9.65×10^9 cm^{-3}

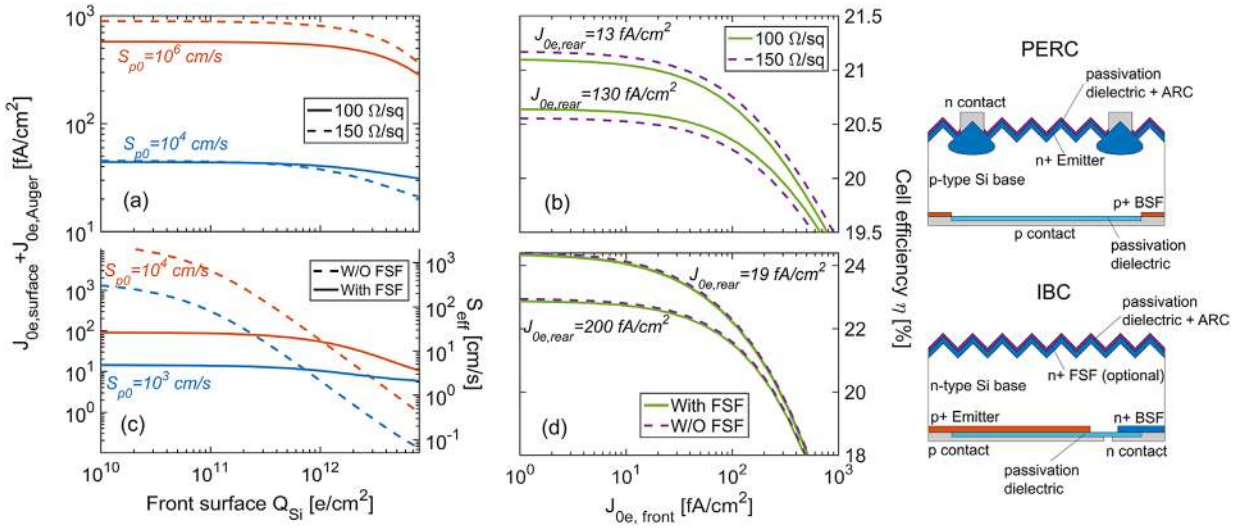

Figure 2 Simulated one-sun performance of the PERC and IBC cells as a function of front surface recombination. (a) EDNA 2 simulated emitter saturation current density for a PERC cell front surface as a function of space-charge-region charge concentration Q_{si}, for two different Erfc emitters with sheet resistance 100 and 150 Ω/□. (b) Quokka simulated PERC cell efficiency as a function of front and back J_{0e} for two conditions of back surface recombination. (c) EDNA 2 simulated emitter saturation current density for an IBC cell front surface as a function of space-charge-region charge concentration Q_{si}, for cells with and without a front surface field. (d) Quokka simulated IBC cell efficiency as a function of front and back J_{0e} for cells with and without a front surface field.

the efficiency dependence on passivation is stronger. The dependence is larger for $J_{0e} > 100\,\text{fA cm}^{-2}$ where losses of over 1% absolute are possible. This is a significant loss in efficiency for a solar cell. This shows that effective passivation schemes for both the front and rear of the cell must be implemented. In the case of this PERC cell, the chemical passivation seems to be the leading mechanism to passivate the front surface. Additionally, improved rear passivation can lead to an increase of over 1% absolute efficiency, if the front surface is optimally passivated. Conversely, for a well passivated rear surface, lighter-doped emitters are beneficial, but heavier-doped emitters are preferred with a poor rear surface. This illustrates the fact that when the rear surface is limiting the performance, the cell benefits from the added conduction in a heavier-doped emitter.

As stated in previous section, higher recombination is typically observed at a textured surface. The front of a solar cell will normally be textured, and the passivation may not be as good as for flat surface. It was noted that, despite the very effective passivation methods review in the next section, the recombination at a textured surface can be over one order of magnitude higher than in a flat surface. This will substantially increase J_{0e}.

For the IBC cell, the large emitter coverage structure A, reported by Reichel et al. [65], was used as a model. Simulations with and without a 200 Ω/□ front surface field were included. The parameters for the modelled IBC cell are listed in Table 1. Figure 2c illustrates a simulation of the J_{0e} parameter conducted in EDNA 2. The effective SRV was calculated using approximation (5) in Ref. [52] for $\Delta n = 10^{15}\,\text{cm}^{-3}$ and is displayed on the right hand y-axis. Here, the presence of a front surface field (FSF) is known to reduce the dependence of surface recombination, and hence J_{0e}, on FEP from dielectric charge. However, in the absence of a FSF, extremely effective passivation can be achieved from FEP with $J_{0e} < 1\,\text{fA cm}^{-2}$. This surface performs better than in the presence of a FSF. This effect is attributed to the Auger recombination in the highly doped region. When chemical passivation is poorer such that surface recombination rates (S_{n0}, S_{p0}) increase, e.g. by an order of magnitude, J_{0e} is seen to increase by approximately the same amount. Field-effect becomes a more relevant passivation mechanism when the chemistry is poor.

Figure 2d illustrates the efficiency of the simulated IBC cell when front surface recombination is varied. The performance of an IBC cell is more strongly dependent on the passivation of its front surface than the PERC cell. This is due to the fact that carriers, normally generated in the near surface region, need to diffuse to the rear emitter before being collected. As the passivation decreases, a steeper dependence is observed. The dependence is particularly strong for $J_{0e} > 100\,\text{fA cm}^{-2}$, leading to large efficiency losses. Improved passivation $J_{0e} < 10\,\text{fA cm}^{-2}$ can lead to an increase of over 1.5% in absolute efficiency (compared to moderate passivation $\sim$100 fA cm^{-2}). Efficiencies exceeding 24% are shown to be possible for this IBC cell when outstanding passivation is provided, $J_{0e} \sim 1\,\text{fA cm}^{-2}$, to both the front and rear of the cell. The rear surface is seen to be of lesser importance in the IBC cell, yet reductions of up to 2% absolute can occur from poor passivation. Despite the passivation benefits of a FSF, it does not improve the carrier conduction. As a matter of fact, for the geometry simulated here the FSF would reduce efficiency marginally

due to the additional Auger recombination in the highly doped front region.

4 Materials and methods for silicon surface passivation

Since the expansion of the silicon solar cell industry in the 1990s, dielectric coatings have been the universal solution to surface passivation and antireflection. Several different technologies have been developed to deposit or grow such dielectric coatings on the cells' surface. An important distinction is now drawn with regard to the passivation quality obtained from the deposition of a dielectric coating. It has been shown that dielectric coatings can change their passivation quality when they are treated after the film has been deposited. This treatment may involve a high-temperature step, e.g. firing of metal contacts in a cell, in either an inert or reactive atmosphere, or the introduction of a secondary passivating species, commonly hydrogen, for additional chemical passivation, or a charged ion for additional field-effect passivation (FEP). In the case of inert anneals, some of the structural properties of the dielectric, especially at the interface with Si, may be modified in a way that both chemical and field-effect passivation are enhanced. In the case of reactive anneals, exposure to hydrogen, or purposeful introduction of species, the surface passivation qualities achieved by the treatment are modified by an external agent, and are thus here termed *extrinsic*. This is as opposed to the *intrinsic* structure and configuration of the interface right after deposition or inert annealing. When reviewing the research on dielectrics for silicon surface passivation, not only the chemical or field-effect components of passivation will be reported, but also the intrinsic and extrinsic origin of such mechanisms.

The materials and deposition methods for surface passivation will be reviewed here chronologically, grouped by the material rather than the deposition technology. The first and most researched dielectric for silicon surface passivation is silicon dioxide (SiO_2). This is thanks to the fact that SiO_2 films allowed the development of MOSFETs in the IC industry during the 1970s and 1980s. After this, the most used and currently standard material for solar cell passivation is silicon nitride (SiN_x). Many combinations of these two have since emerged, and many new materials and methods have been successfully demonstrated to provide outstanding passivation. This review intends to cover those materials and methods developed in the last 20 years. For complimentary reviews covering the advancements in the 1980–1990s, we suggest the work of Aberle [17, 66], and for more recent yet more focussed works see Refs. [67–70]. The subsections to follow concentrate on the S_{eff} metric for the different passivation schemes reviewed, and where data are available a differentiation between chemical and FEP is drawn. At the end of each subsection a summary table of the best performing dielectrics for each deposition or growth technology is provided, and Section 5 summarises all metrics calculated for these passivation dielectrics.

4.1 Silicon oxide

Thermally grown silicon dioxide is among the most ubiquitous dielectric films in semiconductor technology. In the integrated circuit industry this film has been extensively studied and comprehensive summaries can be found in textbooks like Nicollian and Brews [71], Deal and Helms [72] or more recently Engström [73]. In the context of silicon solar cells, on the other hand, the work of Aberle et al. [16, 17, 66, 74, 75] reviews thoroughly the early findings on the passivation quality of SiO_2. As described in his reports, one of the most successful SiO_2 passivation dielectrics is that achieved using the so-called *alneal* process. Kerr and Cuevas [76] reported PC τ_{eff} measurements in such films obtaining what remained the leading passivation scheme during the 2000s. In fact, such was its success that it was used to characterise the Auger and radiative components of bulk recombination in 2002 [77]. When using this process they demonstrated lifetimes as high as 5.25 and 1.65 ms in 1.5 Ωcm n-type and 1 Ωcm p-type material, respectively, equating to SRVs of 1.72 and 7 cm s^{-1}, respectively.

To the authors knowledge, the term *alneal* was coined by Deal in 1970 to refer to aluminium anneals [78, 79]. In this process a thermal SiO_2 film is deposited with a ~0.1–1 μm layer of aluminium, typically using thermal evaporation in vacuum, and then the dielectric is annealed at 400–450 °C in a forming gas (<5% H_2) atmosphere. The benefits of such aluminium or post-metallisation anneal had been known for years [80–88] before Kerr and Cuevas reported its effectiveness using PCD measurements. The widely accepted explanation of the passivation mechanism in *alnealed* samples was first suggested by Balk [80, 81]: during high temperature annealing aluminium reacts with water, probably present in a hydroxyl form, at the oxide surface to form aluminium oxide. This releases hydrogen which quickly diffuses to the Si–SiO_2 interface and passivates some of the harmful bandgap states. The aluminium is then stripped using hot ortho-phosphoric acid rendering the final structure. The change in the electrical properties of the Si–SiO_2 interface due to *alneal* hydrogenation has been thoroughly reported in Ref. [89]. Recently, Collett et al. [90] reported an *enhanced alneal* process whereby charges are introduced into the oxide film at the same time hydrogenation takes place. They demonstrated the introduction of charged ionic species which provide field-effect passivation to the underlying silicon, and reported SRV of 0.5 cm s^{-1} on n-type 1 Ωcm silicon, surpassing that achieved by Kerr and Cuevas. As such, it is clear that both extrinsic chemical and FEP mechanisms can be exploited in *alnealed* SiO_2.

Alnealed SiO_2 has been mainly used in laboratory solar cells, most notably the record-breaking passivated emitter rear locally diffused (PERL) cell, by UNSW [91]. Due to the high temperatures and long timescales it has not been widely adopted in industry. In recent years, however, SiO_2 has gained popularity since it is known to produce the lowest density of interface defect states at the silicon surface. New

implementations include bi- and tri-layers using SiO_2 as the first interfacial layer to silicon, as covered later in this text, or extremely thin oxides where quantum tunnelling effects [92] and/or high density of pinholes [93] aim to provide passivated and carrier selective contacts [94]. Such interest in SiO_2 has motivated new studies where PC lifetime is recorded for different oxidation and extrinsic processing conditions. For example, extrinsic introduction of H has been known for a long time in the form of forming gas anneals (FGA) [95]. Extrinsic modification of the field-effect properties was also proposed long ago using corona discharge [96–98], most notably in the work of Glunz et al. [99]. Most recently Kho et al. [100] demonstrated very effective passivation of oxidised n-type Si using the same technique. It is to note that the stability of many of these extrinsic, both chemical and field-effect, passivation techniques remains an obstacle for adoption into solar cell manufacturing [101, 102], with some progress only recently reported [103]. Despite this, some of the most electrically inactive surfaces have been obtained using such techniques. Bonilla et al. have used corona discharge [104–107] or alkali ionic species [103, 108] to extrinsically charge oxide films and improve their FEP properties. They also performed forming gas anneals to extrinsically incorporate H to the interface and combine it with extrinsic corona FEP [107, 109]. In the best case they reported $\tau_{eff} = 5.13\,ms$, $S_{eff} = 0.24\,cm\,s^{-1}$, in n-type Si 1 Ωcm. When the surface was textured the S_{eff} increased to $28\,cm\,s^{-1}$ [109]. McIntosh and Johnson also observed such increased recombination. They observed 2–12 times higher SRV and attributed it to the increased surface area, dangling bonds and stress-induced defects [55]. Most recently, Hamer et al. [110] and Bourret-Sicotte et al. [111] reported a new methodology to extrinsically introduce H species into a SiO_2 film using a shielded ammonia plasma. By combining extrinsic chemical and FEP of SiO_2 they successfully achieved $\tau_{eff} = 6.4\,ms$, $S_{eff} = 0.17\,cm\,s^{-1}$, in n-type Si 1 Ωcm.

The high temperatures required to grow thermal oxides make it an expensive method for the solar cell industry. Additionally, stability issues and lack of passivation for p-type c-Si have been identified [66, 112]. This resulted in significant efforts being made to develop low-temperature deposition technologies. The most successful of these technologies is plasma-enhanced chemical vapour deposition (PECVD). Hydrogenated silicon sub-oxide (a-SiO_x:H) films were produced using PECVD which led to $\tau_{eff} = 4\,ms$, $S_{eff} = 1.5\,cm\,s^{-1}$, in n-Si 1 Ωcm [113–116]. These required an activation anneal after deposition to reach effective passivation. No in-depth study of the mechanisms has been provided, yet it appears that hydrogenation after deposition plays a vital role in the passivation quality. Other studies focusing on the passivation potential of PECVD SiO_x include Refs. [117–120].

By combining the good intrinsic chemistry in thermal SiO_2, with the hydrogenation from PECVD SiO_x Mack et al. [121] demonstrated SRVs $<10\,cm\,s^{-1}$ in SiO_2/SiO_x double layers. In these kind of films, the main mechanism for passivation was found to be the transport of extrinsic H from the bulk of the film towards the interface. Once there, it chemically passivates the interface dangling bonds during high-temperature treatments [116, 122], like for example forming gas [123] or *alneals* [124, 125]. Similar results have also been achieved using industrial inductively coupled plasma deposition [126, 127], yet insufficient data are available to calculate their metrics for this review.

A recently introduced technique to produce thin dielectric films is atomic layer deposition (ALD). It has gained a lot of attention mainly in the context of aluminium and other metal oxides for passivation. These will be covered in subsequent sections. Here it is noted that SiO_x has been synthesised using the ALD technique yet only moderate passivation has been achieved [128]. Its electrical properties have been recently studied as described in Refs. [129–132].

As the solar cell industry has progressed, it has become a requirement to produce large volumes of cells cost effectively. This has motivated the production of large-throughput dynamic PECVD reactors, much different than the static ones in laboratory facilities. A very complete investigation on PECVD inline production of SiO_x dielectrics has been conducted in recent years by Duttagupta [133]. Along with other reports [134–136], it was demonstrated that only relatively poor passivation is achieved when using such PECVD SiO_x films ($S_{eff} > 100\,cm\,s^{-1}$ in moderately doped silicon) even after temperature treatments and extrinsic H passivation via FGA. To address this issue a second capping layer is commonly deposited on top of an interfacial SiO_x to produce a bilayer stack, typically using silicon nitride (SiN_x) or aluminium oxide (AlO_x) [134, 137]. These multi-layered films will be described later in this paper.

Lastly, it is possible to produce thin oxides using low temperature (<200 °C) chemical methods. These methods have become increasingly important as passivated and electron selective contacts have been demonstrated using a tunnelling ($\sim$1–2 Å) oxide on n-type silicon. The use of a chemically grown tunnelling oxide allowed Fraunhofer ISE to demonstrate over 25% efficient solar cells [138, 139]. An extensive review of chemical SiO_2 methods was provided by Grant and McIntosh [140]. They built on early work of the nitric acid oxidation of silicon (NAOS) technique by Asuha [141] and Mihailetchi [142], to achieve SRVs as low as 20–70 $cm\,s^{-1}$ by constant and alternating voltage anodic oxidation, followed by annealing at 400 °C in oxygen and then forming gas [143–146]. Similar reports by Gad et al. [147] and Stegemann et al. [148] show that a wide range of low temperature chemical oxides present high interface density $\sim 10^{12}\,eV^{-1}\,cm^{-2}$. This leads to relatively poor surface passivation only improved using rapid thermal or forming gas anneals. Other recent reports also make use of light-induced anodisation [149, 150]. In the same manner as PECVD SiO_x, Grant et al. [151] found that the passivation quality and stability of chemically grown oxides could be improved by depositing a SiN_x capping layer. A summary of

the best performing passivating silicon oxide films is shown in Table 2.

4.2 Silicon nitride, oxy-nitrides and stacks The development of low-temperature deposition methods like PECVD enabled extremely effective passivation and antireflection dielectrics, most notably silicon nitride (SiN_x). The seminal work on the electrical properties of the SiN_x–Si interface and its application to solar cells was performed by Schmidt, Kerr, Cuevas, Aberle and Hezel [74, 152–164]. Their advancements made plasma SiN_x into the *de facto* standard film for commercial production of silicon solar cells [2, 165, 166]. Three main advantages have made SiN_x very successful. First, its refractive index is such that the film properties can be tailored to produce excellent antireflection when the cell is encapsulated. Second, PECVD deposition of SiN_x involves the release of large quantities of hydrogen which in turn passivates many surface and bulk defects, both during film deposition and by movement of the H remaining in the film using a post-deposition anneal. And third, the passivation properties of SiN_x can be balanced to jointly exploit the chemical reduction in interface recombination rates, and the field-effect reduction of carrier surface concentration via built-in positive charge. This has been especially effective in highly doped n-type Si which is also the current standard front surface in the vast majority of commercial solar cells.

Table 2 Summary of best performing silicon oxide passivation films for selected growth techniques.

substrate	method – SRV	ref
n-1.5 Ωcm 285 μm	alnealed thermal SiO_2 $^{ExCh,\ St}$ $S_{eff} = 1.72\,cm\,s^{-1}$	Kerr and Cuevas [76]
p-1 Ωcm 400 μm	alnealed thermal SiO_2 $^{ExCh,\ St}$ $S_{eff} = 7.01\,cm\,s^{-1}$	Kerr and Cuevas [76]
n-1 Ωcm 200 μm	enhanced alnealed SiO_2 $^{ExCh,\ St}$ $S_{eff} = 0.44\,cm\,s^{-1}$	Collett [90]
n-1 Ωcm 200 μm	thermal SiO_2 $^{ExFEP,\ St}$ $S_{eff} = 1.45\,cm\,s^{-1}$	Bonilla [107, 109]
n-1 Ωcm 200 μm	FGA thermal SiO_2 $^{ExCh,\ ExFEP,\ St}$ $S_{eff} = 0.24\,cm\,s^{-1}$	Bonilla [107, 109]
n-1 Ωcm 200 μm	SHP thermal SiO_2 $^{ExCh,\ ExFEP,\ St}$ $S_{eff} = 0.17\,cm\,s^{-1}$	Bourret-Sicotte [110, 111]
n-1 Ωcm 250 μm	PECVD a-SiO_x:H $^{ExFEP,\ St}$ $S_{eff} = 1.5\,cm\,s^{-1}$	Mueller [115]
n-5 Ωcm 700 μm	FGA, NAOS SiO_x $^{ExCh,\ St}$ $S_{eff} = 66\,cm\,s^{-1}$	Grant [143, 144]

ExFEP, extrinsically added charge for field-effect passivation; ExCh, extrinsic species added or migrated from to the interface for chemical passivation; St, static deposition method – laboratory facilities.

In these PECVD SiN_x films, the passivation mechanism was identified to be a combination of a slow capture rate at a moderately large concentration of interface states, 10^{11}–$10^{12}\,eV^{-1}\,cm^{-2}$ [167–169], and a high concentration of positive dielectric fixed charged ($\gtrsim 10^{12}\,e/cm^2$) repelling holes from the surface [167, 168, 170, 171]. PECVD allows control of the concentration of reactant precursors so that the film's stoichiometry can be adjusted. For SiN_x, silicon-rich films lead to a film structure very similar to amorphous silicon, where passivation is mainly provided by the chemical reduction in recombination rates. For a nitrogen-rich film, on the other hand, chemical passivation is reduced and field-effect passivation is enhanced by the formation of silicon-nitrogen dangling bonds, i.e. a silicon atom backbonded to three nitrogens ($\bullet SiN_3$) [171–177]. This defect is known as the K centre and presents an amphoteric nature – i.e. it can change its charge state between neutral, positive and negative depending on the Fermi level [178]. K centres in SiN_x are typically positively charged. Progress in the past two decades developed an optimal combination of these two factors leading to outstanding passivation using PECVD SiN_x films. Kerr and Cuevas [160] achieved S_{eff} of 7 and $14\,cm\,s^{-1}$ for 1.5 Ωcm n- and 1 Ωcm p-type silicon, respectively. Improvements to such work followed soon after by Chen et al. [179–181] who produced S_{eff} of $1.38\,cm\,s^{-1}$ in 1 Ωcm n-type Si, and by Richter et al. [41] who reported $0.64\,cm\,s^{-1}$ in silicon of the same kind and resistivity. Most recently, Wan et al. [182, 183] reported one of the lowest SRVs of PECVD SiN_x, $0.67\,cm\,s^{-1}$ in 0.85 Ωcm p-type Si, and immeasurably low SRV on 0.47 Ωcm n-type, with the additional advantage of very low optical absorption. On a textured surface, Wan and McIntosh [184] showed that SRV could increase by a factor of ~1.8 for silicon-rich films, or ~6 for nitrogen rich films, when the larger surface area of a pyramidal surface is not accounted for, as noted in Section 2. For a thorough review of the electronic properties of these films see Aberle's book [17].

It is evident that extensive work has resulted in extremely effective plasma nitride films. To complement these advances, high throughput industrial tools have been developed, where dynamic deposition allows inline manufacture of solar cells. Some studies investigated these industrial techniques yet with limited success [185–189]. The work of Duttagupta [133] covers the most substantial progress in this area. He found S_{eff} under 1.82 and $2.46\,cm\,s^{-1}$ in 1 Ωcm n- and p-type Si using nitride films deposited in industrial scale inline PECVD reactors. In similar studies Duttagupta et al. [133, 170, 190] investigated the passivation mechanisms of these films and found that the effectiveness of passivation was mainly due to the field-effect repulsion of carriers from an intrinsic fixed charge concentration of $3–5 \times 10^{12}\,q/cm^2$. A smaller effect due to the chemical component was suggested.

When examining the results obtained for both SiO_2 and SiN_x films, in this and the previous subsection, it becomes evident that the electrical characteristics that each film

provide are somewhat complimentary. While SiO_2 films present the lowest interface state density D_{it}, which in many cases transfers into very low interface capture velocities S_{n0}, S_{p0}, their counterpart SiN_x films exhibit a large concentration of charge that provides effective FEP. In fact, researchers realised early on that, when depositing a PECVD SiN_x film, a very thin interfacial oxy-nitride gets formed, abbreviated SiO_x:N_y, or SiON for short. Aberle [177] reported that such a layer forms due to the very thin native SiO_x film that grows on the surface between cleaning steps and the start of the deposition process. This understanding brought about the implementation of double-layered stacks consisting of an intentional SiO_2 or SiO_x film, complemented by a second SiN_x film providing the same three advantages mentioned earlier, yet with the possibility of even better passivation quality. This concept has been exploited by many researchers in the past decades. By using an initial thermally grown oxide and subsequent PECVD SiN_x Schmidt et al. [159, 161], and later Mack et al. [121, 191] demonstrated S_{eff} in the range ~5–10 cm s^{-1} in ~1 Ωcm p-type Si. In n-type silicon, where passivation is more effective, Larionova et al. [192] demonstrated a S_{eff} of 0.42 cm s^{-1}, and Bonilla et al. [193] obtained 0.17 cm s^{-1}, for 2.5 and 1 Ωcm resitivities, respectively. They reported that the mechanisms involved in such good passivation were a combination of the intrinsic field-effect due to grown-in charge in the nitride layer, the extrinsic chemical passivation of the Si–SiO_2 interface (due to hydrogen ingress during PECVD deposition of the nitride), and the subsequent addition of extrinsic field-effect via corona discharge [193, 194]. When used on a textured surface, Bonilla et al. [102] reported a S_{eff} of 34 cm s^{-1} in an as deposited oxide-nitride stack, and 14 cm s^{-1} after extrinsic addition of charge. Some other works have also used native [195] and rapid thermal oxides [196–199] as the first layer under a SiN_x film, yet their results are not as effective as those using high temperature ones.

The higher speed and lower temperature of PECVD systems have made plasma SiO_x a suitable choice as the first layer in oxide-nitride stacks. Early works by Chen et al. reported the benefits of the second SiN_x capping layer [123]. The nitrides not only provided better passivation but also improved the stability of oxide films. Work of Hofmann et al. [69, 200, 201] and Dingemans et al. [137] demonstrated that despite the initially poor intrinsic qualities of a PECVD SiO_x film, extrinsic improvement is possible from hydrogenation during nitride deposition and/or post-deposition activation anneals. Additionally, the nitride film has an intrinsic concentration of fixed charge which provides FEP. While Hofmann et al. achieved SRVs in the ~40 cm s^{-1} range for p-type Si, Dingemans et al. improved upon this work and showed S_{eff} of 7.6 cm s^{-1} in n-type Si 3.5 Ωcm, and 11.2 cm s^{-1} in p-Si 2 Ωcm. Using second-harmonic generation spectroscopy they demonstrated that the SiO_x/SiN_x double layer stack exhibits lesser charge than a single SiN_x film, yet enough to contribute some FEP. The key component of passivation, however, is that achieved by the low recombination rates due to hydrogenation of the interface states [137]. Other authors have also reported the use of such passivation approaches in actual solar cells [202, 203], with some issues noted during post-deposition annealing or firing steps [204]. All oxide-nitride double layer films reviewed until now have been deposited using laboratory scale PECVD. As noted earlier, this is not well suited for large scale production. Practical manufacturing of solar cells requires dynamic fast deposition of dielectrics. Duttagupta addressed this using inline PECVD deposition of oxide-nitride stacks [133]. He demonstrated that optimal SiO_x/SiN_x films could be produced in fast inline reactors reaching S_{eff} of 8.15 cm s^{-1} on n-type Si 1.5 Ωcm, and 35 cm s^{-1} in p-type Si 1.5 Ωcm [134, 205, 206].

The last nitride dielectric system reviewed in this section is that obtained when oxygen is present during deposition. Plasma processing where both oxygen and nitrogen precursors are present gives rise to a new dielectric material commonly termed silicon oxy-nitride (SiON). Despite their wide range of applications in the IC industry [207–209], SiON films have only recently been applied to silicon cell surface passivation. As mentioned earlier, it had been suggested that the thin native oxide film is normally turned into a SiON upon plasma deposition of SiN_x, or during oxidising treatments afterwards. The studies of Lepinski et al. [210], Dupui et al. [211–213] and Seiffe et al. [214, 215] appear to be the earliest reports of an intentionally grown SiON film in the context of silicon solar cells. Seiffe et al. achieved the most promising results. They studied the electrical properties of this film and found that, when capped with a second SiN_x film, the SiON-SiN_x double layer stack not only provides excellent passivation, but also resists the high and rapid temperature processing that solar cells commonly undergo after dielectric deposition. They found that S_{eff} below 1.35 and 2.85 cm s^{-1} were possible in n- and p-type 1 Ωcm silicon. Achieving such excellent passivation required activation steps using a high temperature firing at ~650 °C, and light soaking. In addition to PC lifetime measurements, Seiffe et al. used a combination of surface photo-voltage, capacitance voltage measurements and electron paramagnetic resonance to study the mechanisms of passivation. They found a large concentration of a fixed dielectric positive charge. They proposed that this charge originates from shallow donor states in the SiON layer, presumably arising from over-coordinated oxygen and/or nitrogen atoms in the silicon network, which were likely formed as their film was silicon rich. They also find that despite the large concentration of dielectric charge, only part of it is mirrored in the silicon space charge region. This indicated that a large concentration of interface states is present and charged. The chemical component of passivation was studied in lesser detail yet it is reasonable to assume a contribution from hydrogenation during SiN_x deposition and H migration during firing. From their work it appears

intrinsic and extrinsic components of passivation are present and combined in this SiON–Si interface.

Subsequent studies have explored this dielectric system in more detail. Laades et al. [216] and Shwab et al. [217] corroborated previous findings on the thermal stability of SiON films, and additionally showed that H passivation played a key role in the passivation properties upon high-temperature firing. Zhou et al. [218, 219] systematically studied the plasma deposition parameters, while Brinkmann et al. [220] investigated the films' electrical, optical and structural properties. They found optimal conditions for passivation with results similar to Seiffe's. Also, SiON films were shown resistant to a well-known deterioration effect termed potential induced degradation (PID) – a decrease in cell performance due to changes in the passivation dielectric from high voltage differences to the module frame [219, 221, 222]. Similar preliminary findings in the same system were previously reported by Zhu et al. [223]. Work of Cheng et al. [224] also found that the chemical passivation component played a more important role after firing the SiON/SiN_x stack, and similar stability and passivation effectiveness was shown. Hallam et al. [225] showed that the passivation provided by SiON was strongly dependent on it composition, with low N–H bond density providing optimal results. In addition to PECVD, atmospheric pressure [226], and expanding thermal plasma methods have been explored but only poor passivation was achieved [227]. Modest passivation has also been achieved using sputtered SiN_x [228, 229]. Lastly, it is noted that these oxy-nitride systems have been successfully used to passivate the rear (normally p-type) surface of silicon solar cells, e.g. Refs. [230, 231]. A summary of the best performing passivating silicon nitride films is shown in Table 3.

Table 3 Summary of best performing silicon nitride passivation films for selected deposition techniques.

substrate	method – SRV	ref
n-1.5 Ωcm 305 μm	PECVD SiN_x^{St} $S_{eff} = 7.06\,cm\,s^{-1}$	Kerr and Cuevas [160]
p-1 Ωcm 400 μm	PECVD SiN_x^{St} $S_{eff} = 14.8\,cm\,s^{-1}$	Kerr and Cuevas [160]
n-1 Ωcm 240 μm	PECVD SiN_x^{St} $S_{eff} = 1.38\,cm\,s^{-1}$	Chen [180, 181]
n-1 Ωcm 200 μm	PECVD SiN_x^{St} $S_{eff} = 0.64\,cm\,s^{-1}$	Richter [41]
p-0.85 Ωcm 295 μm	PECVD SiN_x^{St} $S_{eff} = 0.67\,cm\,s^{-1}$	Wan [182]
n-1 Ωcm 280 μm	inline PECVD SiN_x^{Dy} $S_{eff} = 3.83\,cm\,s^{-1}$	Duttagupta [133]
p-1 Ωcm 280 μm	inline PECVD SiN_x^{Dy} $S_{eff} = 4.11\,cm\,s^{-1}$	Duttagupta [133]
p-1 Ωcm 400 μm	thermal SiO_2-PECVD SiN_x^{St} $S_{eff} = 8.6\,cm\,s^{-1}$	Schmidt [121, 161]
n-2.5 Ωcm 155 μm	thermal SiO_2-PECVD SiN_x^{St} $S_{eff} = 0.42\,cm\,s^{-1}$	Larionova [192]
n-1 Ωcm 200 μm	thermal SiO_2-PECVD SiN_x^{St} $S_{eff} = 0.17\,cm\,s^{-1}$	Bonilla [193]
n-3.5 Ωcm 280 μm	PECVD SiO_x/SiN_x^{St} $S_{eff} = 7.6\,cm\,s^{-1}$	Dingemans [137]
p-2 Ωcm 280 μm	PECVD SiO_x/SiN_x^{St} $S_{eff} = 11.2\,cm\,s^{-1}$	Dingemans [137]
n-1.5 Ωcm 150 μm	inline PECVD SiO_x/SiN_x^{Dy} $S_{eff} = 8.15\,cm\,s^{-1}$	Duttagupta [133]
p-1.5 Ωcm 160 μm	inline PECVD SiO_x/SiN_x^{Dy} $S_{eff} = 35.6\,cm\,s^{-1}$	Duttagupta [205]
n-1 Ωcm 250 μm	PECVD SiON/SiN_x^{Dy} $S_{eff} = 1.35\,cm\,s^{-1}$	Seiffe [214]
p-1 Ωcm 205 μm	PECVD SiON/SiN_x^{Dy} $S_{eff} = 2.85\,cm\,s^{-1}$	Seiffe [214]

St, static deposition method – laboratory facilities; Dy, dynamic deposition method – industrial.

4.3 Amorphous silicon and associated stacks Sanyo, now owned by Panasonic, developed the heterojunction silicon solar cell in the 1980–1990s [232]. Their successful Heterojunction with Intrinsic Thin layer (HIT) concept brought attention to the singular properties of the amorphous-crystalline silicon (a-Si/c-Si) interface [233, 234]. It was demonstrated that this heterojunction could conduct one type of carrier while limiting the recombination losses typical of metal-semiconductor contacts [235, 236]. This allowed a cell architecture with outstanding open circuit voltages, and efficiencies as high as 25% [10]. When used in a cell, however, multi-layered and doped a-Si films are required [10, 237, 238]. This allows charge carrier collection in the cell. Such systems are beyond the scope of this paper. Here, the properties of undoped or intrinsic a-Si will be reviewed in the context of surface passivation (minority carrier) rather than carrier conductivity (majority carrier).

a-Si is a semiconductor, thus its use as a passivation material requires a second, and in some cases, a third layer. These provide both antireflection and insulation properties to the surface. This subsection examines the electrical characteristics of such dielectric systems, focusing on the mechanisms of passivation provided by the a-Si/c-Si interface.

Early studies on recombination at the a-Si/c-Si interface were limited [239, 240], or mainly related to the HIT cell architecture [241, 242]. They reported relatively poor SRVs

in the 50–100 cm s^{-1} range [243]. The first extensive work including PC measurements of a-Si passivation was that of Dauwe et al. [243–245]. They found that SRVs approaching 10 cm s^{-1} were possible in n- and p-type, moderately doped silicon. One of the main advantages inherited from HIT cell processing is the low-temperature deposition. In Dauwe's studies, the films were deposited below 250 °C using PECVD. From the point of view of solar cell manufacturing this has two benefits. Firstly, it allows cheaper manufacture of cells because of the lower thermal budget. Secondly, it eases the requirement for clean processing since impurities will not diffuse into the silicon at this low temperature.

Further studies of a-Si followed. Those of Olibet, De Wolf and Ballif [237, 246–254] significantly progressed the understanding of the a-Si/c-Si interface electrical properties. They introduced a model to describe its recombination. In it, interface dangling bonds were represented as amphoteric defects. Using this description they successfully modelled injection-dependent recombination at the a-S/c-Si interface, which they proposed was governed by the density and the charge state of such amphoteric centres [250]. Similarly to the SRH theory, passivation was achieved by a reduction in the concentration of amphoteric centres, and a reduction in one type of carrier using field-effect. In studies by the same group, Descoeudres et al. [255] found that extrinsic hydrogenation could be used to improve the interface. It should be noted that a-Si films are often deposited from precursors already containing H. Such films are commonly termed hydrogenated amorphous silicon and abbreviated as a-Si:H. Olibet et al. [249] reported SRVs as low as 7.6 and 14.4 cm s^{-1} in n- and p-type silicon, 2.5 Ωcm. This was improved by Schüttauf et al. [256] who reported SRV nearing 1 cm s^{-1} in similar material, and by Strahm et al. [257] who reported 1.2 cm s^{-1} in 4 Ωcm n-type Si. In the former, data were not available to calculate the metrics for this review.

In these interfaces, an atomically abrupt interface was shown to be a prerequisite for good passivation. They were able to tune the FEP properties of this interface by applying a subsequent doped amorphous or microcrystalline Si film, and found a more symmetric capture velocity for electrons and holes at the a-Si/c-Si interface, as compared to SiO_2 [16] and SiN_x [154]. Regarding the energy band structure of the a-Si/c-Si junction, asymmetric band offsets were found such that holes tend to face a larger barrier than electrons [258, 259]. In the more common {111} texture Si surface, they found that a-Si films still performed well. Stegemann et al. [260] showed that the pyramid size influenced the passivation quality of a-Si films, yet Muñoz et al. [261] and Angermann et al. [262] showed that optimal texturing leads to a negligible loss in surface passivation, and Descoeudres et al. [263] reported the best performing a-Si passivation in textured silicon with $S_{eff} = 7.6$ and 14.4 cm s^{-1} in n- and p-type, 4 Ωcm. One limiting factor in the application of a-Si to solar cells is optical parasitic absorption. Wan et al. [264] addressed this by producing sub-nm a-Si layers capped with SiN_x.

The lowest observed recombination at the a-Si/c-Si interface has been that reported by Herasimenka et al. [265] and Bonilla et al. [266]. Herasimenka demonstrated SRVs of 0.086 cm s^{-1} in 1.7 Ωcm n-type Si, while Bonilla achieved 0.06 cm s^{-1} in 1 Ωcm n-type Si. They demonstrated such inactive surfaces by combining the excellent a-Si/c-Si chemical interface, with enhanced FEP from corona discharge. The a-Si layer and its hydrogenation during plasma deposition of SiO_x/SiN_x provided the chemical component. Such correlation of passivation and H content has been studied in detail by De Wolf [247, 252, 253] and Nakada [267], while the effect of film morphology on the H dynamics was addressed by Gerke et al. [268]. Bonilla et al. [266] attributed the chemical component of passivation to a reduced hole capture rate rather than fewer interface states. The presence of oxide and nitride capping layer(s) has been shown beneficial not only to improve passivation, but also thermal stability [269–273]. This is mainly attributed to preventing hydrogen out-effusion from the a-Si. Some changes in the field-effect passivation properties have also been reported to occur during post-deposition heat treatments [274]. Lastly, the need for wafer pre-cleaning or preconditioning was noted in [275], and some success has also been achieved using other CVD deposition techniques [276–280]. Only the work of Koyama et al. [281] resulted in very effective passivation using hot-wire CVD a-Si/SiN_x films, with SRV in the ~2 cm s^{-1} range.

In summary, a-Si films provide four main advantages to other passivation schemes: first a-Si has an energy band structure which, when abrupt interfaces are achieved, produces a sharp energy step at both the conduction and valence band edges with those of c-Si. This prevents carriers from reaching harmful states in the a-Si bulk. Second a-Si deposition involves large quantities of hydrogen which contribute to passivate its bulk, interface states, and defects in the c-Si. Third, while the recombination of minority carriers is prevented by this film, majority carrier conduction is possible as seen in the HIT cell concept. And lastly, the deposition temperature of these films is substantially lower than that commonly used in cell manufacturing, allowing reductions in thermal budget and lesser cleanliness requirements. Successful application of a-Si films to different cell architectures has continued to expand as for example noted in Refs. [237, 255, 263, 282–287]. The main disadvantage of a-Si films is, however, the sensitivity to subsequent high-temperature processes which are often required in industrial manufacturing technology. A summary of the best performing passivating amorphous silicon films is shown in Table 4.

4.4 Aluminium oxide and stacks The development of aluminium oxide (AlO_x) surface layers is one of the main breakthroughs in surface passivation in the past two decades. In the 1980s Hezel and Jäger [158, 288] first demonstrated a reasonable level of passivation using AlO_x. They achieved SRVs in the ~100 cm s^{-1} region on p-type Si. However, they only used it in the context of

Table 4 Summary of best performing amorphous silicon passivation films and associated stacks, for selected deposition techniques.

substrate	method – SRV	ref
n-2.5 Ωcm 275 μm	VHF-PECVD a-SiSt $S_{eff} = 7.6\,cm\,s^{-1}$	Olibet [249]
p-2.5 Ωcm 275 μm	VHF-PECVD a-SiSt $S_{eff} = 14.4\,cm\,s^{-1}$	Olibet [249]
n-4 Ωcm 230 μm, T	VHF-PECVD a-SiSt $S_{eff} = 0.8\,cm\,s^{-1}$	Descoeudres [263]
p-4 Ωcm 230 μm, T	VHF-PECVD a-SiSt $S_{eff} = 3.1\,cm\,s^{-1}$	Descoeudres [263]
n-4 Ωcm 280 μm	PECVD a-SiSt $S_{eff} = 1.2\,cm\,s^{-1}$	Strahm [257]
n-1.7 Ωcm 300 μm	PECVD a-Si/SiO_x/$SiN_x$$^{St,\ ExFEP,\ ExCh}$ $S_{eff} = 0.086\,cm\,s^{-1}$	Herasimenka [265]
n-1 Ωcm 200 μm	PECVD a-Si/SiO_x/$SiN_x$$^{St,\ ExFEP,\ ExCh}$ $S_{eff} = 0.06\,cm\,s^{-1}$	Bonilla [266]

T indicates a textured substrate. ExFEP, extrinsically added charge for field-effect passivation; ExCh, extrinsic species added or migrated from to the interface for chemical passivation; St, static deposition method – laboratory facilities.

inversion-layer metal-insulator-semiconductor (IL-MIS) solar cells [288]. The work of König and Ebest [289] then explored the characteristics of this insulator and its potential for electron devices. They remarked on its concentration of negative charge [290], as opposed to positively charged SiO_x and SiN_x. The major advanceme took place when, almost simultaneously, Agostinelli et al. [291, 292] and then, Hoex et al. [293–295] reported AlO_x films synthesised via the atomic layer deposition (ALD) technique. These films achieved SRVs nearing $10\,cm\,s^{-1}$ in both n- and p-type silicon, making them rapidly popular. In addition to the excellent passivation, the fact that they are negatively charged made them especially suited for p-type surfaces since they would not induce inversion layers that could lead to shunting losses at the solar cell level [296, 297]. This was especially important as p-type silicon surfaces are key in the more efficient cell architectures, for example in n-type Local-BSF cells with a passivated front boron emitter [298], or p-type PERC cells with the rear p-surface passivated, which are now being adopted industrially [284]. In AlO_x films tailoring the charge has also been reported [299]. Small negative charge concentrations can be produced which makes them also suitable for n-type surfaces.

The seminal work of Agostinelli and Hoex was rapidly expanded. Most notably, the studies of Benick and Richter [41, 298, 300–306], Dingemans et al. [307–314] and Saint-Cast et al. [296, 315–318], largely advanced the understanding of the electrical properties of the film, its passivation effectiveness, and its application to silicon solar cells. A key aspect of the passivation achieved using AlO_x is the requirement for an activation step. Annealing for 10–30 min at temperatures between 350 and 450 °C, in an inert or forming gas environment, has been found to activate the passivation [309, 310]. The effect this has is both related to chemical and field-effect passivation in the film. Before these mechanisms are described it is important to note the four main techniques used to deposit AlO_x. Two kinds of ALD deposition have been developed. One in which the substrate temperature provides the energy to drive the reaction, and thus may require higher temperatures and longer times, and another where a plasma activates and accelerates the reaction [319, 320]. They are termed thermal and plasma ALD, respectively. The third technique is the well-known PECVD, the fourth is atmospheric pressure chemical vapour deposition (APCVD), and last, sputtering.

In thermal ALD an initially good chemical passivation is marginally improved upon annealing, while the FEP is greatly improved [321, 322]. In plasma ALD the initial chemical passivation is poorer, presumably due to plasma radiation and ion bombardment during deposition, but it improves, on annealing, to values similar to those for the thermal process [300, 303, 307, 323]. The FEP in this case improves by a small amount. In PECVD AlO_x, Saint-Cast [315] found similar results to the case of plasma ALD. Poor initial chemical passivation in this film could be improved using post-deposition anneal (~450 °C) or firing (~850 °C) steps, whilst FEP due to negative charge was only moderately improved. In all cases, the FEP relates to a high concentration ($\sim -10^{12}$ to $-10^{13}\,e/cm^2$) of negative charge [294, 296, 324]. Similar to the case of SiN_x films, a thin SiO_x interfacial layer is normally formed during the deposition of AlO_x films. This was reported by Hoex et al. [293, 294] and corroborated by Verlaan et al. [325] in the context of Si surface passivation. The formation of dielectric charge seems related to point defects at the SiO_x/AlO_x interface produced during deposition, and charged via injection from the c-Si. This was concluded from second-harmonic generation measurement in varying thickness samples [312]. The negative charge concentration was found invariable across different thicknesses in AlO_x films [326, 327]. It is thus concluded that the FEP mechanism in these films is intrinsic to the structure of the c-Si/SiO_x/AlO_x interfaces.

With regards to chemical passivation, deep level transient spectroscopy (DLTS) [328], electron spin resonance (ESR) [329], and electrically detected magnetic resonance (EDMR) [309, 330] measurements, revealed that the interface presents the same P_b centres and E'-like defects as a c-Si/SiO_2 interface. This correlates well with the presence of the interfacial SiO_x that forms during deposition. On the other hand, the large concentration of atomic H in the as-deposited state of these films has been found the main contributor to the improvement in chemical

passivation upon temperature treatment. The concentration of defects at the c-Si/SiO_x interface is largely decreased upon such annealing. This indicates that the chemical component of passivation in this film originates from the extrinsic hydrogen species migrating from the bulk of the film towards the interface. Passivation stability has been found dependent on the structure of the film [311], yet remarkably stable structures have been reported [301, 306, 309]. A more detailed description of these mechanisms, the deposition technology, and the application of AlO_x-based passivation to solar cells can be found in Dingemans and Kessels' 2012 review paper [309].

The best performing AlO_x passivation film has been demonstrated by Richter et al. [41] using plasma ALD. They showed that S_{eff} as low as 0.26 and 0.95 cm s^{-1}, respectively, was possible on n- and p-type Si, 1 Ωcm. It is noted that this level of passivation is exceptional, yet very effective passivation with SRVs in ~1 cm s^{-1} has now been routinely demonstrated using both thermal and plasma ALD, for example in the work of Dingemans and Liao [307, 310, 331]. An advantage of ALD AlO_x deposition is the fact it is normally done at temperatures between 150 and 250 °C [309]. As mentioned for a-Si films, this is beneficial for industrial production. Its main disadvantage, on the other hand, is the deposition speed. For the industrial production of solar cells high throughput techniques are required. To address this issue batch process chambers have been proposed [309], but most notably, a new deposition ALD concept was developed and dubbed spatial-ALD [332–334]. In this method the two half-reactions that normally take place in an ALD system are separated spatially rather than temporarily. This method proved similarly effective and is now a proven industrial technology [309, 335].

A more commonly used method for high-volume manufacturing is PECVD. Passivation quality comparable to that of ALD can be achieved in PECVD AlO_x films. Miyajima et al. [336] reported moderate passivation using this technique, but it was Dingemans et al. [314] who demonstrated efficient passivation with S_{eff} of 0.45 cm s^{-1} in 3.5 Ωcm n-type Si. In both cases they used a static reactor designed for laboratory research with a deposition rate of ~5–10 nm min^{-1}. Saint-Cast et al. [296] first showed a S_{eff} of 7.47 cm s^{-1} in 1 Ωcm p-type Si using a fast inline reactor. Duttagupta [133, 299] followed and achieved S_{eff} of 1.4 cm s^{-1} in 3 Ωcm n-type Si, and 15 cm s^{-1} in 3.5 Ωcm p-type Si, using inline PECVD deposition of AlO_x. This demonstrates that sufficient passivation can be achieved in high throughput techniques using AlO_x films. In their studies, Saint-Cast [315] and Duttagupta [133] also showed that a second (capping) layer deposited on top of AlO_x brings a number of benefits. The relative expensive AlO_x layer could be made thinner, better antireflection could be achieved when applied to the cells front surface, additional hydrogenation could be obtained, and better stability to cell firing steps and chemical metal pastes could be achieved. However, despite the additional hydrogenation, the passivation quality improved marginally with a second PECVD SiO_x or SiN_x capping layer.

Different to the case of ALD AlO_x, in PECVD films both the chemical and field-effect components of passivation develop during post-deposition anneal or firing. Saint-Cast et al. [318] and Duttagupta [133] used surface photo-voltage experiments to characterise the interface state density and film charge concentration. They observed a reduction in the interface state density, and an increase in the dielectric built-in charge upon heat treatment after deposition. A practical example of such a heat treatment could be that given during the deposition of a second capping layer, or an intentional anneal or firing step. Other studies corroborating such findings include Refs. [313, 337–339]. This indicates the field-effect passivation in these films is produced by an intrinsic change in the defect structure at the AlO_x/SiO_x/c-Si interfaces, while the chemical passivation is provided by the extrinsic migration of hydrogen from the bulk of the film towards the interface. These studies also corroborated the presence of a thin interfacial SiO_x at the PECVD AlO_x/c-Si region. In fact, other works have intentionally grown a SiO_x layer using thermally grown [311, 340], and low temperature wet [341], ALD [342] or CVD [135] techniques, which are then capped with an AlO_x layer to produce high levels of passivation, and improve the stability of SiO_x films. The best results were obtained by Dingemans on thermal SiO_2 [340] and ALD SiO_2 [342], capped with ALD AlO_x. He reported SRVs ~3.6 cm s^{-1} on 2–3 Ωcm n-type silicon. The mechanisms of passivation were similar to those on single AlO_x layer, with the advantage that the negative charge built at the SiO_x/AlO_x interface exceeds the positive charge at the SiO_x/Si interface, making this structure suitable to passivate n-type and p-type silicon surface simultaneously [343].

The need for fast industrial methods has driven research into new deposition methods for AlO_x. Most recently, Black [344] produced a comprehensive study of AlO_x films using atmospheric pressure chemical vapour deposition (APCVD). He demonstrated that extremely high-quality passivation can be achieved by a high-throughput and industrially compatible method. This is of importance as atmospheric methods are easily implemented in inline manufacturing, and are thus more cost-effective. Black achieved SRVs as low as 2.32 cm s^{-1} on 1.2 Ωcm n-type Si, and 4.37 cm s^{-1} on 1.35 Ωcm p-type Si. In the APCVD case, the passivation was activated using post-deposition firing and illumination steps. The degree of chemical and field-effect passivation changed in the same manner as for PECVD films with both chemistry and charge concentration improving on activation. Black et al. [345, 346] also reported similarly efficient passivation using rapid thermal annealing, or SiN_x capping layers. A summary of the best performing passivating aluminium oxide films is shown in Table 5.

4.5 Titanium oxide Titanium oxide (TiO_x) was the antireflection coating of choice when production of silicon

Table 5 Summary of best performing aluminium oxide passivation films and associated stacks, for selected deposition techniques.

substrate	method – SRV	ref
n-1.9 Ωcm 275 μm	plasma ALD $AlOx^{St,\ ExCh}$ $S_{eff} = 1.4\,cm\,s^{-1}$	Hoex [293, 295]
n-1 Ωcm 200 μm	plasma ALD $AlOx^{St,\ ExCh}$ $S_{eff} = 0.26\,cm\,s^{-1}$	Richter [41]
p-1 Ωcm 200 μm	plasma ALD $AlOx^{St,\ ExCh}$ $S_{eff} = 0.95\,cm\,s^{-1}$	Richter [41]
n-2.5 Ωcm 280 μm	thermal ALD $AlOx^{St,\ ExCh}$ $S_{eff} = 1.23\,cm\,s^{-1}$	Liao [331]
n-3.5 Ωcm 280 μm	PECVD $AlO_x^{St,\ ExCh}$ $S_{eff} = 0.45\,cm\,s^{-1}$	Dingemans [314]
p-1 Ωcm 250 μm	inline PECVD $AlO_x^{Dy,\ ExCh}$ $S_{eff} = 7.47\,cm\,s^{-1}$	Saint-Cast [296]
n-3 Ωcm 120 μm	inline PECVD $AlO_x^{Dy,\ ExCh}$ $S_{eff} = 1.4\,cm\,s^{-1}$	Duttagupta [133]
p-3.5 Ωcm 160 μm	inline PECVD $AlO_x^{Dy,\ ExCh}$ $S_{eff} = 15\,cm\,s^{-1}$	Duttagupta [133]
n-1.2 Ωcm 300 μm	inline APCVD $AlO_x^{Dy,\ ExCh}$ $S_{eff} = 2.32\,cm\,s^{-1}$	Black [344]
p-1.35 Ωcm 435 μm	inline APCVD $AlO_x^{Dy,\ ExCh}$ $S_{eff} = 4.37\,cm\,s^{-1}$	Black [344]
n-2 Ωcm 200 μm	thermal $SiO_x/AlOx^{St,\ ExCh}$ $S_{eff} = 3.62\,cm\,s^{-1}$	Dingemans [340]

ExCh, extrinsic species added or migrated from to the interface for chemical passivation; St, static deposition method – laboratory facilities.

solar cells increased in the 1980–1990s [347–349]. This was due to its versatility and low cost. TiO_x showed optimal optical properties to act as an antireflection coating between a silicon surface and an Ethylene Vinyl Acetate (EVA) encapsulant film used when packing cells into modules [350]. The ideal refractive index for the top antireflection layer in encapsulated cell is ~2.1 at $\lambda = 630$ nm [351]. Deposition of TiO_x was performed using either chemical [352] or physical vapour techniques [350], and its use extended beyond that of the solar industry, most prominently in glass manufacturing as a protection coating deposited using ultra-high throughput techniques [353, 354]. Despite its ideal optical properties, TiO_x was replaced by hydrogenated silicon nitride (SiN_x) since the evolution of silicon solar cells required appropriate passivation of the cells front surface, and this could not be accomplished using TiO_x [355]. As mentioned in previous sections, PECVD SiN_x is today's preferred method to provide passivation and antireflection to the cell front surface. However, it has a number of weaknesses. Firstly, it requires a vacuum for the film deposition process, secondly, it typically presents a concentration of positive charge thus being less efficient at passivating p-type surfaces, thirdly, it has a practical maximum refractive index of ~2.1 due to high optical absorption losses in Si-rich films [161, 162], thus being a less ideal ARC between silicon and EVA, and lastly, the precision and sensitivity of inline PECVD deposition leads to a trade-off between the optical and passivation properties achieved in a single film.

In recent years, interest in TiO_x has re-emerged since its electrical properties are now starting to show promise. Several dielectric deposition methods have been used in the past to deposit TiO_x, however, only recently Thomson and McIntosh [356] demonstrated reasonable surface passivation using low-temperature APCVD. In their work, they report moderate levels of passivation when TiO_x coated Si is subjected to anneal and light soaking steps. They achieved SRVs in the ~30 cm s^{-1} range for 5 Ωcm n-type silicon. Liao et al. [357, 358] later showed excellent passivation of both n- and p-type silicon using TiO_x films, yet they synthesised the films using ALD. S_{eff} values of 3.22 and 8.9 cm s^{-1} were achieved on 2.5 Ωcm n-type and 2 Ωcm p-type silicon. Cui et al. [359] not only reported excellent passivation of ALD TiO_x with SRV below 6.72 cm s^{-1} in 1 Ωcm n-type silicon, but also showed its application to boron diffused emitters in PERC cells, achieving efficiencies over 20%. All these studies also indicated that TiO_x is negatively charged. This explained its better suitability to passivate p-type silicon.

In previous sections, it was shown that the passivation quality of many dielectric coatings can be modified by

Table 6 Summary of best performing titanium oxide passivation films and associated stacks, for selected deposition techniques.

substrate	method – SRV	ref
n-5 Ωcm 430 μm	APCVD $TiO_x^{Dy,ExCh}$ $S_{eff} = 29.6\,cm\,s^{-1}$	Thomson and McIntosh [356]
n-2.5 Ωcm 280 μm	ALD $TiO_x^{St,\ ExCh}$ $S_{eff} = 3.22\,cm\,s^{-1}$	Liao [357]
p-2 Ωcm 280 μm	ALD $TiO_x^{St,\ ExCh}$ $S_{eff} = 8.91\,cm\,s^{-1}$	Liao [357]
n-1 Ωcm 180 μm	ALD $TiO_x^{St,\ ExCh}$ $S_{eff} = 7.62\,cm\,s^{-1}$	Cui [359]
n-1 Ωcm 100 μm	thermal SiO_2 – APCVD $TiO_x^{Dy,\ ExFEP}$ $S_{eff} = 3.88\,cm\,s^{-1}$	Bonilla [360]

ExFEP, extrinsically added charge for field-effect passivation; ExCh, extrinsic species added or migrated from to the interface for chemical passivation; St, static deposition method – laboratory; Dy, dynamic deposition method – industrial.

deposition of a second film, or by processing the film after deposition. Bonilla et al. [360] reported effective passivation in a double layer coating consisting of thermal SiO_2 and APCVD TiO_x. They showed S_{eff} of 3.88 cm s^{-1} in 1 Ωcm n-type silicon when the film was extrinsically charged using corona. In particular they showed that the films optical properties can be tailored in APCVD deposition, as previously shown by Davis et al. [351], while passivation properties are modified post-deposition by additional processing. A summary of the best performing passivating titanium oxide films is shown in Table 6.

4.5 Silicon carbide A less widely investigated but moderately effective passivation film is amorphous silicon carbide (SiC_x). This film is rarely used at the solar cell device level, yet it is included here for completeness. The work of Martin et al. [361–365] largely looks at the electrical characteristics of the PECVD SiC_x–Si interface and its application to silicon solar cells. Similar to previously reviewed dielectrics, SiC_x films benefit from post-deposition activation anneals. This effect is likely due to the migration of H from the bulk of the film to the interface with Si. Intrinsic and hydrogenated SiC_x has been shown to provide SRVs of ~30 cm s^{-1} on 3.3 Ωcm, p-type Si [363]. When doped with phosphorus, however, the SRV can be improved to 2–4 cm s^{-1} on 1 Ωcm, p-type Si [366]. In both cases, the highest quality passivation has been observed in silicon-rich films. The passivation mechanism is thus quite similar to a-Si:H [362]. Compared to a-Si, the advantage of SiC_x films is their tuneable bandgap in the range of 1.5–3 eV. This results in a reduced parasitic absorption and it is thus preferable to a-Si [367–370]. Stacks of a-Si and SiC_x on solar cells have also been investigated as a means to reduce the degradation of a-Si passivation at elevated temperature [370, 371]. Although typically deposited using a CVD technique [362, 363, 372], surface passivation using SiC_x has also been explored on physical vapour deposition (PVD) techniques, such as sputtering [373, 374].

Combined antireflection and passivation has been also reported on PECVD silicon carbo-nitrides (SiC_xN_y) [362, 364, 365, 375, 376]. SRVs in the range of ~3–6 cm s^{-1} on 1 Ωcm silicon, n-type and p-type have been achieved using SiC_xN_y films [362]. However, films that provided effective passivation did not have suitable optical parameters. Instead, double layer stacks have been proposed to achieve both passivation and antireflection [362, 364]. For example, SiC_x has been used as the capping layer of AlO_x [377]. The passivation in this case is attributed to both FEP, caused by the negative charge of the AlO_x, and hydrogenation during the SiC_x:H deposition. Silicon carbide layers have also been used in conjunction with SiN_x as a passivation and anti-reflection coating [378] where the majority of passivation was provided by the inherent charge of the SiN_x. Solar cells featuring SiC_x rear surface passivation were reported to 20.2% efficiency [69, 379]. Although moderately effective, the SiC_x passivation does not yet compete with the schemes previously reviewed.

4.7 New metal oxides In the past few years novel metal oxide structures have been researched with the aim of understanding better the mechanisms of passivation and carrier conduction. Most prominently, crystalline silicon surface passivation has been reported for hafnium oxide (HfO_x), gallium oxide (GaO_x) and tantalum oxide (TaO_x).

HfO_x films synthesised via ALD have recently gained attention since, besides passivating, they also provide good antireflection and firing stability to the silicon surface [380, 381]. Early works showed moderate passivation of both n- and p-type silicon [380, 382–385], yet only recently Cheng et al. [386] reported a S_{eff} of 7 cm s^{-1} in n-type 2.8 Ωcm Si deposited with HfO_x and anneal-activated. Only a day later Cui et al. [387] reported a yet better performing HfO_x film, with a S_{eff} of 1.9 and 7.3 cm s^{-1} in n- and p-type 1 Ωcm silicon. In their best performing sample, both Cheng and Cui, measured a low interface state density of $<10^{11}$ eV^{-1} cm^{-2}, probably related to H migration during the anneal, and a moderate positive charge concentration in the dielectric ($1–5 \times 10^{11}$ e/cm^2). This would indicate that the mechanism of passivation is mainly chemical in origin. No report of capture rates has been produced yet but it is likely that those states at the HfO_x/Si interface are not very recombination active, such that the good passivation is explained. The negative charge developed seems to originate by intrinsic structural changes in the film, near the HfO_x/Si interface, which also has been reported to have an interfacial SiO_x present [380].

The work of Allen and Cuevas [388–391] shows the first surface passivation application of ALD GaO_x for solar cells.

Table 7 Summary of new metal oxide passivation films.

substrate	method – SRV	ref
n-2.8 Ωcm 280 μm	ALD $HfO_x^{St, ExCh}$ $S_{eff} = 7$ cm s^{-1}	Cheng [386]
n-1 Ωcm 205 μm	ALD $HfO_x^{St, ExCh}$ $S_{eff} = 1.92$ cm s^{-1}	Cui [387]
p-1 Ωcm 198 μm	ALD $HfO_x^{St, ExCh}$ $S_{eff} = 7.29$ cm s^{-1}	Cui [387]
p-1.6 Ωcm 260 μm	ALD $GaO_x^{St, ExCh}$ $S_{eff} = 2.84$ cm s^{-1}	Allen [390]
n-1 Ωcm 390 μm	ALD TaO_x – PECVD $SiN_x^{St, ExCh}$ $S_{eff} = 3.32$ cm s^{-1}	Wan [392]
p-0.8 Ωcm 275 μm	ALD TaO_x – PECVD $SiN_x^{St, ExCh}$ $S_{eff} = 4.85$ cm s^{-1}	Wan [392]

ExCh, extrinsic species added or migrated from to the interface for chemical passivation; St, static deposition method – laboratory facilities.

They found that, similar to AlO_x and HfO_x ALD films, GaO_x is negatively charged. Upon a post-deposition activation anneal they found a very low interface state density ($<10^{11}\,eV^{-1}\,cm^{-2}$) and a large concentration of negative charge ($10^{12}\,e/cm^2$). With such films they demonstrated a S_{eff} of 2.84 cm s^{-1} in p-type 1.6 Ωcm silicon. It appears both chemical and field-effect mechanisms are active. No studies have been reported on the capture rates at these interface states, and no conclusions can be drawn from the data reported so far. Lastly, improved stability to firing and additional hydrogenation was found when a second SiN_x capping layer was deposited [390].

Wan et al. [392, 393] first explored the use of ALD TaO_x films to passivate a silicon surface. They showed that by capping the TaO_x film with a PECVD SiN_x, a negatively charged passivation stack could be produced. Charge densities in excess of $-10^{12}\,e/cm^2$ were demonstrated. No analysis of the interface state density has been provided to date but there appears to be an interfacial layer with properties different to the commonly observed SiO_x film [392]. S_{eff} of 3.32 and 4.85 cm s^{-1} was inferred for n- and p-type 1 Ωcm silicon featuring the ALD TaO_x-PECVD SiN_x stack.

Lastly, a very recent report by Repo et al. [394] has shown that ALD aluminium nitride films have the potential to passivate the silicon surface. No data was available to calculate the metrics for this review yet a SRV in the order of 80 cm s^{-1} was reported with a large concentration of interface states and positive dielectric charge. A summary of the best performing passivating metal oxide films is shown in Table 7.

5 Summary and discussion This review has presented the advancements in dielectric surface passivation for silicon solar cells over the past two decades. Comparing the passivation performance in different dielectrics has been largely hindered by the many different metrics and analysis methods provided in the literature. This has been addressed here by processing all photoconductance measurements of $\tau_{eff}(\Delta n)$ reported in the literature using the same methodology. In the previous section, the surface recombination velocity has been calculated using such methodology, and it was used as the main indicator of passivation effectiveness. However, it is convenient to measure the performance of the different materials and deposition methods using the four metrics described in Section 2: τ_{eff}, S_{eff}, J_{0s}, iV_{oc}. Figure 3

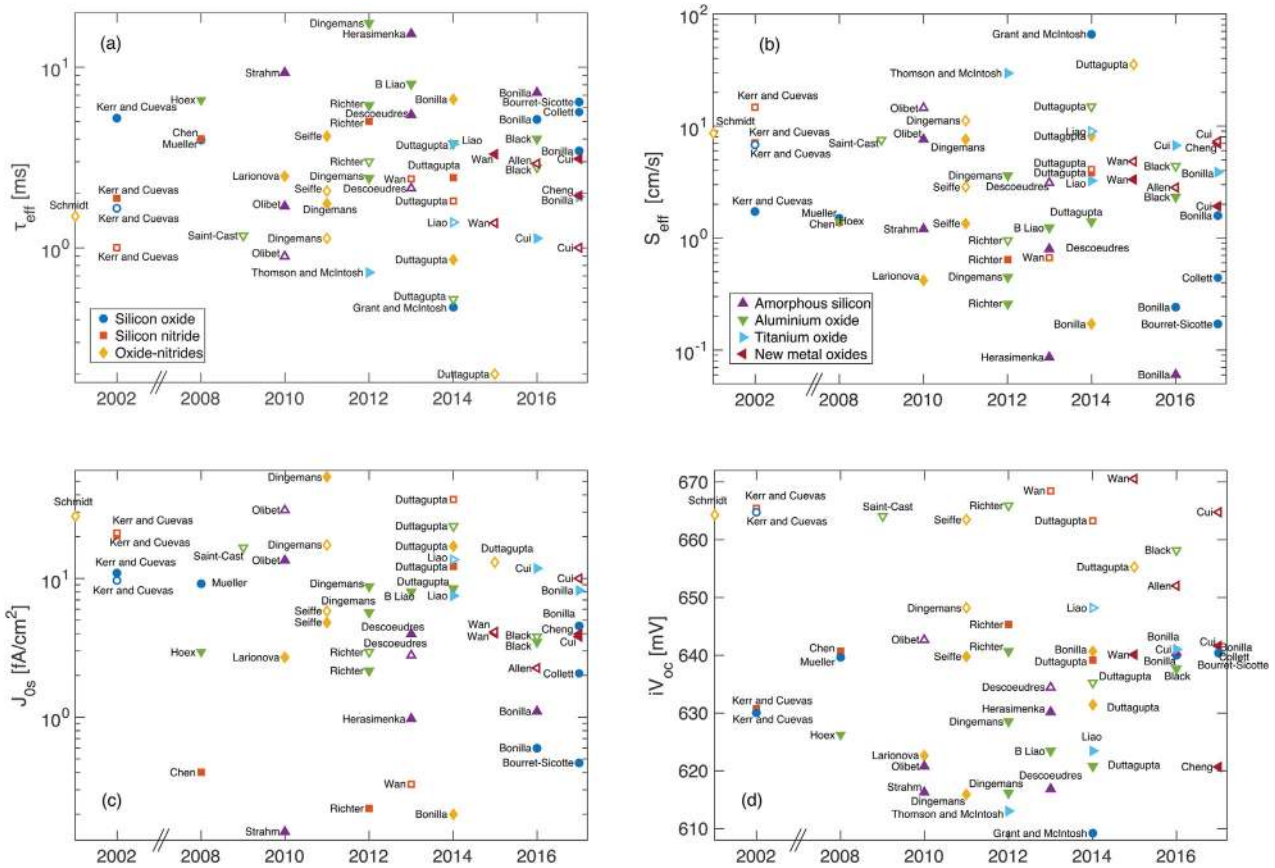

Figure 3 Surface passivation metrics for dielectric coatings developed over the past two decades, for n-type (closed symbols) and p-type (open symbols) silicon surfaces. Details on the substrate and deposition technique are provided in Tables 2–7. All values of S_{eff}, τ_{eff} and iV_{oc} are given at $\Delta n = 10^{15}\,cm^{-3}$, and calculated directly from reported PC $\tau_{eff}(\Delta n)$ measurements. All substrates are {100} orientation.

Table 8 Summary of techniques used to grow or deposit passivation dielectrics.

deposition	material	merits	demerits	references
thermal growth	SiO_2	effective passivation of both *n* and *p* silicon	requires temperatures >800 °C	[16, 177, 405]
		very low interface state density $10^{10}\,eV^{-1}\,cm^{-2}$	slow growth	
		batch processing	minimal field-effect passivation	
		suitable refractive index for rear surface	positive dielectric charge $\sim 10^{11}\,e/cm^2$	
			unsuitable refractive index for front ARC	
anodic oxidation	SiO_x	low temperature <100 °C	poor chemical passivation	[143–146]
		fast ($\sim$100 nm min^{-1})	negligible field-effect	
		controllable thin oxide thicknesses	only thin layers possible	
		improved interface upon deposition of 2nd layer	not suitable for front ARC	
		allows tailoring 2nd layer intrinsic charge	electrochemical process difficult to implement industrially	
direct, static PECVD	SiN_x	low temperature <500 °C	lack of passivation of *p* silicon	[17, 152–164]
		moderate deposition rate ($\sim$10 nm min^{-1})		
		very effective passivation of *n* silicon		
		moderate interface state density $10^{11}\,eV^{-1}\,cm^{-2}$		
		high concentration of (+) charge $10^{12}\,e\,cm^{-2}$		
		hydrogenation during and after deposition		
		suitable refractive index for front surface		
	SiO_x	temperature and speed	poor chemical and FEP when used alone. Moderate to high interface state density $10^{12}\,eV^{-1}\,cm^{-2}$ without hydrogenation	[113–116]
		improved interface upon deposition of 2nd layer or hydrogenation anneal		
		allows tailoring of intrinsic dielectric charge		
		suitable refractive index for rear surface		
	a-Si	temperature and speed	moderate to high interface state density $>5\times10^{11}\,eV^{-1}\,cm^{-2}$	[249, 257, 263]
		effective passivation of both *n* and *p* silicon		
		extremely low recombination rates due to hydrogenated defects		
	AlO_x	temperature and speed	lack of passivation of *n* silicon	[314, 336]
		effective passivation of *p* silicon		
		moderate interface state density $10^{11}\,eV^{-1}\,cm^{-2}$		
		high density of negative charge $>10^{12}\,e/cm^2$		
		hydrogenation during and after deposition		
		does not require activation		

(*Continued*)

Table 8 (*Continued*)

deposition	material	merits	demerits	references
		anneal suitable refractive index for rear surface		
remote PECVD	SiN_x	better passivation than direct systems very low interface state density $10^{10}\,eV^{-1}\,cm^{-2}$ high concentration of (+) charge $\sim 10^{12}\,e\,cm^{-2}$	slow deposition when used in an inline system results are variable and typically not optimal	[153, 170]
inline PECVD	SiO_x	low temperature $<500\,^{\circ}C$ fast ($>100\,nm\,min^{-1}$) industrial facilities	poor chemical and FEP when used alone moderate to high interface state density $10^{12}\,eV^{-1}\,cm^{-2}$ and lack of FEP	[133–136]
	SiN_x	temperature, speed, industrial effective passivation of *n* silicon moderate interface state density $10^{11}\,eV^{-1}\,cm^{-2}$ high concentration of (+) charge $10^{12}\,e\,cm^{-2}$ hydrogenation during and after deposition	lower effectiveness than static methods	[133, 170, 190]
	AlO_x	temperature, speed, industrial effective passivation of both *p* silicon moderate interface state density $10^{11}\,eV^{-1}\,cm^{-2}$ high density of negative charge $>10^{12}\,e/cm^2$ hydrogenation during and after deposition does not require activation anneal	lower effectiveness than static methods	[133, 296, 299]
thermal ALD	AlO_x	extremely high passivation of *n* and *p* silicon low interface state density $<10^{11}\,eV^{-1}\,cm^{-2}$ high concentration of (−) charge $>10^{12}\,e/cm^2$ low temperature $<300\,^{\circ}C$	requires a post-deposition anneal slow deposition rates $<10\,nm\,min^{-1}$ better suited for *p* than *n* silicon	[309]
	TiO_x	effective passivation of both *p* and *n* silicon low temperature $<250\,^{\circ}C$ negatively charged	slow deposition rates $<10\,nm\,min^{-1}$ requires thermal and light soaking activation	[357–359]
	HfO_x	effective passivation of both *p* and *n* silicon low temperature $<400\,^{\circ}C$ moderate negative charge concentration in the dielectric $1–2\times10^{11}\,e/cm^2$ possible hydrogenation	slow deposition rates $<10\,nm\,min^{-1}$ better suited for *p* than *n* silicon requires thermal activation	[386, 387]
	GaO_x	low temperature $<300\,^{\circ}C$ effective chemical and FEP of *p* silicon very low interface state density $<10^{11}\,eV^{-1}\,cm^{-2}$ large negative charge	slow deposition rates $<10\,nm\,min^{-1}$ not reported on *n* silicon	[390]

(*Continued*)

Table 8 (*Continued*)

deposition	material	merits	demerits	references
		$>10^{12}$ e cm^2		
		can be improved upon SiN_x capping layer		
	TaO_x	effective passivation of *p* silicon upon SiN_x	slow deposition rates <10 nm min^{-1}	[392, 393]
		large negative charge $\sim10^{12}$ e/cm^2	requires a PECVD SiN_x second layer	
plasma ALD	AlO_x	extremely high passivation of *n* and *p* silicon	requires a post-deposition anneal	[309]
		low interface state density $<10^{11}$ eV^{-1} cm^{-2}	slow deposition rates <10 nm min^{-1}	
		high concentration of (−) charge $>10^{12}$ e cm^{-2}	not industrial applicable	
		low temperature <300 °C	better suited for *p* than *n* silicon	
		lower temperature than thermal ALD		
		better quality than thermal ALD		
spatial ALD	AlO_x	equivalent to thermal ALD	lower passivcation quality than achieved with spatial ALD	[309]
		demonstrated industrial capability		
APCVD	AlO_x	low temperatures <500 °C	lower quality than ALD	[344, 345]
		fast (>100 nm min^{-1})	better suited for *p* than *n* silicon	
		industrial facilities		
	TiO_x	low temperatures <500 °C	poor passivation quality	[356, 360]
		fast (>100 nm min^{-1})	requires underlying film	
		industrial facilities		
		ideal refractive index for front surface		
sputtering	AlO_x	low temperature <50 °C	requires extrinsic hydrogenation	[406, 407]
		negatively charged	lower quality	
		industrially scalable but slow deposition		
	a-Si	low temperature <400 °C	requires extrinsic hydrogenation	[408]
		industrial facilities	lower quality than PECVD	
		industrially scalable but slow deposition		

illustrates the surface passivation metrics for the highest performing passivation dielectrics. Only the most effective material for each deposition or growth technique has been included. Tables 2–7 provide the information on the deposition techniques and substrates.

A few materials and techniques can be highlighted in reference to Tables 2 to 7 and Fig. 3. Very high levels of c-Si surface passivation by SiO_2 and SiN_x were demonstrated early on thanks to the work of Kerr, Cuevas and Schmidt. PECVD then rapidly became the technique of choice and extremely well-passivated surfaces were possible with oxides and nitrides. PECVD additionally extended the possible material systems, mainly allowing deposition of multiple layer stacks, and the very effective a-Si and AlO_x films. The emergence of ALD provided a new tool to explore dielectric thin films. It became rapidly popular and proved advantageous in the developments of AlO_x by Agostinelli, Hoex and Dingemans. Extrinsic passivation has been shown to improve most films significantly, however, its practical application to commercial manufacture relies on its stability with respect to other cell processing steps, e.g. firing, and to the cell operation conditions, e.g. UV radiation. The extrinsic addition of hydrogen species has been shown to be one of the most successful methods to improve passivation effectiveness. It can be achieved using an external H source, during deposition of a film with H containing precursors, or on an activation anneal after a hydrogenated film is deposited. The stability of hydrogenation has been achieved using two or three capping layers on the initial dielectric-silicon interface. The stability of field-effect passivation, on the other hand, has been explored in less detail. Intrinsic dielectric charge is mainly due to structural changes that take place during deposition or activation steps. These would appear stable to firing and

radiation in SiN_x [201, 273] and AlO_x films [309]. The stability of extrinsic charge, such as corona and/or ionic charge, has only recently been studied. Corona charges have long been known to provide poor stability, which can be moderately improved with a hydrophobic chemical treatment of the interface [109, 395]. Better results have been achieved when large alkali ions are introduced into the dielectric coating as demonstrated with potassium in SiO_2 [108], thus bringing extrinsic FEP methods closer to practical implementation. Lastly, surface passivation research in recent years has concentrated on two aspects. First bringing the extraordinary performance of laboratory-scale material systems to industrial scale deposition techniques. And secondly, on the exploration of new material systems, mainly metal oxides using the ALD technique, to address some of the shortfalls of the established SiN_x and emergent AlO_x films.

In this review, the focus was placed on the materials used to produce effective surface passivation of silicon. Each material can be deposited using different deposition techniques. Although these techniques have been covered in the text, a summary of how they compare was not provided. Such comparison is now provided in Table 8. Here, a list of all the main deposition or growth techniques is provided, and each material–technique combination is assessed on the merits and demerits previously reviewed. It is clear that while silicon oxide provides outstanding chemical passivation, the charge concentration provided by other materials and deposition techniques makes them preferable. Additionally, a continuous progression towards methods and materials which can be implemented industrially is evidenced. As such, thin and low-temperature oxides, and inline PECVD oxides and nitrides, are preferred due to their high throughput, despite their currently lower performance. Lastly, the emergence of ALD has allowed a wider range of materials to be explored, and outstanding passivation provided.

The cell architecture where these dielectrics are of interest must also be taken into account. The PERC-type architecture, including PERL and PERT, and the back contact architecture, including IBC cells, are predicted to dominate the market in the coming decades. Excellent passivation will be required for rear p-type surfaces in PERC cells, front n-type surfaces in IBC cells, and simultaneous rear p^+ and n^+ surfaces in IBC cells. Additionally, for front surface films, adequate optical properties will be necessary. That is, neglible parasitic absorption, and a refractive index to match the EVA encapsulant ($\sim$2.3). In the simulations in Section 3, the focus was placed on n-type surfaces, which typically benefit from positive charge. However, it is clear that both p and n surfaces are present at cell level, and thus films where charge can be tailored to either polarity, or to negligible values, are more versatile and desirable to enhance cell performance. All the factors described here must be taken into account when selecting a suitable passivation methodology for front and rear cell surfaces.

6 Outlook Silicon surface passivation has been widely researched in the past decades. Vast improvements have taken place and SRV values approaching zero have been shown possible. Such exceptional performance has been possible in very carefully optimised dielectric coatings at laboratory scale. A large number of methods have been proposed and researched. Deposition of dielectric coatings with optimal intrinsic passivation has been combined with extrinsic ways of improving their performance. Adaptation of these methods depends on compatibility with efficient and industrially adopted cell architectures, thus scalability to mass production and stability to cell manufacturing processes and under cell operating conditions.

Thanks to laboratory research, many such improvements in passivation have been successfully transferred into industrial techniques, and applied to solar cell manufacturing. Every relevant surface can now be passivated with surface recombination currents in the low single digits, and very effective passivation has already been implemented industrially. The gap between large-scale and laboratory-scale results is continuously closing, and very good passivation dielectrics are already possible for the current level of efficiency in solar cells. As other loss mechanisms of the cells are reduced, the surface will require further passivation.

Current research on interface phenomena has shifted to new directions. The exceptional performance from the passivation dielectrics reviewed here shows that very little room for improvement is possible. New perspectives include methods that not only minimise recombination of the minority carrier, but also improve the conduction of the majority carrier. This novel and recent concept is described as selective and passivated contacts. They make use of dielectric coatings that can preferentially conduct one type of carrier while providing the best possible passivation to the opposite type. In this area, the understanding of surface passivation (minimal minority carrier concentration) is a pre-requisite to the successful application of dielectrics to carrier selective and passivated contacts. The most notable advancements in this new area is reported in the work of Bullock, Wan, Allen and Cuevas [2, 396–400], Feldmann, Reichel, Hermle and Glunz [138, 139, 401], Brendel [402] and Stradins [403, 404].

Acknowledgements RS Bonilla is the recipient of an EPSRC (UK) Postdoctoral Research Fellowship, EP/M022196/1. PR Wilshaw and P Hamer acknowledge the support from EPSRC grant EP/M024911/1. Data published in this article can be downloaded from http://ora.ox.ac.uk.

References

[1] M. A. Green, K. Emery, Y. Hishikawa, W. Warta, E. D. Dunlop, D. H. Levi, and A. W. Y. Ho-Baillie, Prog. Photovolt. Res. Appl. **25**, 3–13 (2017).
[2] C. Battaglia, A. Cuevas, and S. De Wolf, Energy Environ. Sci. **9**, 1552–1576 (2016).
[3] International Energy Agency, Technology Roadmap: Solar Photovoltaic Energy – 2016 Edition, Paris, France, 2014.

[4] Fraunhofer ISE, Photovoltaics Report, Freiburg, 2016.
[5] M. J. (Mariska) de Wild-Scholten, Energy payback time and carbon footprint of commercial photovoltaic systems, Sol. Energy Mater. Sol. Cells. **119**, 296–305 (2013). https://doi.org/10.1016/j.solmat.2013.08.037
[6] M. A. Green, Nature Energy **1**, 15015 (2016).
[7] D. M. Powell, M. T. Winkler, H. J. Choi, C. B. Simmons, D. B. Needleman, and T. Buonassisi, Energy Environ. Sci. **5**, 5874 (2012).
[8] A. C. Goodrich, D. M. Powell, T. L. James, M. Woodhouse, and T. Buonassisi, Energy Environ. Sci. **6**, 2811 (2013).
[9] K. Yoshikawa, H. Kawasaki, W. Yoshida, T. Irie, K. Konishi, K. Nakano, T. Uto, D. Adachi, M. Kanematsu, H. Uzu, and K. Yamamoto, Nature Energy **2**, 17032 (2017).
[10] K. Masuko, M. Shigematsu, T. Hashiguchi, D. Fujishima, M. Kai, N. Yoshimura, T. Yamaguchi, Y. Ichihashi, T. Mishima, N. Matsubara, T. Yamanishi, T. Takahama, M. Taguchi, E. Maruyama, and S. Okamoto, IEEE J. Photovolt. **4**, 1433–1435 (2014).
[11] Fraunhofer ISE (2017).
[12] W. Shockley and W. T. Read, Phys. Rev. **87**, 835–842 (1952).
[13] R. N. Hall, Phys. Rev. **87**, 387 (1952).
[14] D. J. Fitzgerald and A. S. Grove, Surf. Sci. **9**, 347–369 (1968).
[15] R. B. M. Girisch, R. P. Mertens, R. F. Dekeersmaecker, and R. F. De Keersmaecker, IEEE Trans. Electron Dev. **35**, 203–222 (1988).
[16] A. G. Aberle, S. Glunz, and W. Warta, J. Appl. Phys. **71**, 4422–4431 (1992).
[17] A. G. Aberle, Crystalline Silicon Solar Cells: Advanced Surface Passivation and Analysis (UNSW, Sydney, Australia, 2009).
[18] A. Cuevas and D. Yan, IEEE J. Photovolt. **3**, 916–923 (2013).
[19] A. Cuevas, T. Allen, and J. Bullock, 2015 IEEE 42nd Photovolt. Spec. Conf. (2015), pp. 1–6.
[20] W. Shockley and G. L. Pearson, Phys. Rev. **74**, 232–233 (1948).
[21] W. Shockley, Electrons and Holes in Semiconductors: With Applications to Transistor Electronics (D. Van Nostrand Company, Inc., New York, 1950).
[22] K. R. McIntosh and L. E. Black, J. Appl. Phys. **116**, 14503 (2014).
[23] F.-J. Ma, S. Duttagupta, K. D. Shetty, L. Meng, G. S. Samudra, B. Hoex, and I. M. Peters, J. Appl. Phys. **116**, 184103 (2014).
[24] A. S. Grove and D. J. Fitzgerald, Solid. State. Electron. **9**, 783–806 (1966).
[25] D. R. Lillington and G. F. J. Garlick, in: 18th IEEE Photovolt. Spec. Conf., 1985, p. 1677.
[26] J. C. Jimeno, A. Cuevas, and A. Luque, in: 18th IEEE Photovolt. Spec. Conf., 1985, p. 726.
[27] B. Knobloch, J. Aberle, A. G. Warta, and W. Voss, in: 8th Eur. Photovolt. Sol. Energy Conf. (Kluwer Academic Press, 1988), pp. 1165–1170.
[28] D. T. Stevenson and R. J. Keyes, J. Appl. Phys. **26**, 190–195 (1955).
[29] S. Deb and B. R. Nag, J. Appl. Phys. **33**, 1604–1604 (1962).
[30] M. Kunst and G. Beck, J. Appl. Phys. **60**, 3558–3566 (1986).
[31] P. A. Basore, B. R. Hansen, in: IEEE Conf. Photovolt. Spec., IEEE, n.d., pp. 374–379.
[32] H. W. Curtis and R. L. Verkuil, Lifetime Factors Silicon, ASTM STP 712, 1980, pp. 210–224.
[33] T. Tiedje, J. I. Haberman, R. W. Francis, and A. K. Ghosh, J. Appl. Phys. **54**, 2499–2503 (1983).
[34] E. Yablonovitch, D. L. Allara, C. C. Chang, T. Gmitter, and T. B. Bright, Phys. Rev. Lett. **57**, 249–252 (1986).
[35] D. E. Kane and R. M. Swanson, in: Proc 18th IEEE Photovolt. Spec. Conf., 1985, pp. 578–583.
[36] E. Yablonovitch and T. J. Gmitter, Solid. State. Electron. **35**, 261–267 (1992).
[37] R. A. Sinton and A. Cuevas, Appl. Phys.Lett. **69**, 2510 (1996).
[38] R. A. Sinton, A. Cuevas, and M. Stuckings, in: Photovolt. Spec. Conf. 1996. Conf. Rec. Twenty Fifth IEEE, 1996, pp. 457–460.
[39] www.sintoninstruments.com (2017).
[40] S. M. S. Sze, N. Kwok Kwok, and K. K. Ng, Physics of Semiconductor Devices, Third Ed. (John Wiley and Sons, Inc., Hoboken, New Jersey 2007).
[41] A. Richter, S. W. Glunz, F. Werner, J. Schmidt, and A. Cuevas, Phys. Rev. B **86**, 165202 (2012).
[42] P. P. Altermatt, F. Geelhaar, T. Trupke, X. Dai, A. Neisser, and E. Daub, in: NUSOD '05. Proc. 5th Int. Conf. Numer. Simul. Optoelectron. Devices, 2005, IEEE, n.d., pp. 47–48.
[43] T. Trupke, M. A. Green, P. Würfel, P. P. Altermatt, A. Wang, J. Zhao, and R. Corkish, J. Appl. Phys. **94**, 4930 (2003).
[44] N. E. Grant, F. E. Rougieux, D. Macdonald, J. Bullock, and Y. Wan, J. Appl. Phys. **117**, 55711 (2015).
[45] N. E. Grant, F. E. Rougieux, and D. Macdonald, Solid State Phenom. **242**, 120–125 (2015).
[46] N. E. Grant, V. P. Markevich, J. Mullins, A. R. Peaker, F. Rougieux, and D. Macdonald, Phys. Status Solidi RRL **10**, 443–447 (2016).
[47] A. Kimmerle, J. Greulich, and A. Wolf, Sol. Energy Mater. Sol. Cells **142**, 116–122 (2015).
[48] K. L. Luke and L.-J. Cheng, J. Appl. Phys. **61**, 2282 (1987).
[49] A. B. Sproul, J. Appl. Phys. **76**, 2851 (1994).
[50] D. B. M. Klaassen, Solid. State. Electron. **35**, 961–967 (1992).
[51] www.pvlighthouse.com.au (2017).
[52] H. Mäckel and K. Varner, Prog. Photovolt. Res. Appl. **21**, 850–866 (2013).
[53] R. Pässler, Phys. Rev. B **66**, 85201 (2002).
[54] A. Cuevas and R. A. Sinton, Prog. Photovolt. Res. Appl. **5**, 79–90 (1997).
[55] K. R. McIntosh and L. P. Johnson, J. Appl. Phys. **105**, 124520 (2009).
[56] S. C. Baker-Finch and K. R. McIntosh, IEEE J. Photovolt. **1**, 59–65 (2011).
[57] A. Kimmerle, M. Momtazur Rahman, S. Werner, S. Mack, A. Wolf, A. Richter, and H. Haug, J. Appl. Phys. **119**, 25706 (2016).
[58] M. Edwards, S. Bowden, U. Das, and M. Burrows, Sol. Energy Mater. Sol. Cells **92**, 1373–1377 (2008).
[59] ITRPV, Technology Roadmap: Solar Photovoltaic Energy − 2016, n.d.
[60] K. R. McIntosh, P. P. Altermatt, M. D. Abbott (2017).
[61] A. Fell, IEEE Trans. Electron Dev. **60**, 733–738 (2013).

[62] A. Fell, K. R. McIntosh, P. P. Altermatt, G. J. M. Janssen, R. Stangl, A. Ho-Baillie, H. Steinkemper, J. Greulich, M. Muller, B. Min, K. C. Fong, M. Hermle, I. G. Romijn, and M. D. Abbott, IEEE J. Photovolt. **5**, 1250–1263 (2015).
[63] P. A. Basore and K. Cabanas-Holmen, in: 27th Eur. Photovolt. Sol. Energy Conf. Exhib. (2012), pp. 1462–1464.
[64] P. A. Basore and D. A. Clugston, PC1D – (n.d.).
[65] C. Reichel, F. Granek, M. Hermle, and S. W. Glunz, Prog. Photovolt. Res. Appl. **21** (2012).
[66] A. G. Aberle, Prog. Photovolt. **8**, 473–487 (2000).
[67] M. Z. Rahman and S. I. Khan, Mater. Renew. Sustain. Energy **1**, 1 (2012).
[68] J. Schmidt, F. Werner, B. Veith, D. Zielke, S. Steingrube, P. P. Altermatt, S. Gatz, T. Dullweber, and R. Brendel, Energy Procedia **15**, 30–39 (2012).
[69] M. Hofmann, S. Janz, C. Schmidt, S. Kambor, D. Suwito, N. Kohn, J. Rentsch, R. Preu, and S. W. Glunz, Sol. Energy Mater. Sol. Cells **93**, 1074–1078 (2009).
[70] N. Balaji, S. Q. Hussain, C. Park, J. Raja, J. Yi, and R. Jeyakumar, Trans. Electr. Electron. Mater. **16**, 227–233 (2015).
[71] E. H. Nicollian and J. R. Brews, MOS (Metal Oxide Semiconductor) — Physics and Technology (Wiley, New York, 1982).
[72] B. E. Deal and C. Helms, The Physics and Chemistry of SiO2 and the Si-SiO2 Interface (Springer US, New York, 1993).
[73] O. Engström, The MOS System (Cambridge University Press, Cambridge, 2014).
[74] J. Schmidt, T. Lauinger, A. G. Aberle, and R. Hezel, in: Conf. Rec. Twenty Fifth IEEE Photovolt. Spec. Conf. – 1996, IEEE, 1996, pp. 413–416.
[75] A. Aberle, S. Glunz, and W. Warta, Sol. Energy Mater. Sol. Cells **29**, 175–182 (1993).
[76] M. J. Kerr and A. Cuevas, Semicond. Sci. Technol. **17**, 35–38 (2002).
[77] M. J. Kerr and A. Cuevas, J. Appl. Phys. **91**, 2473 (2002).
[78] B. E. Deal, in: Symp. Silicon Device Process. Vol. 13, 1970, pp. 36–50.
[79] P. L. Castro and B. E. Deal, J. Electrochem. Soc. **118**, 280 (1971).
[80] P. Balk, in: Electrochem. Soc. Meet. Buffalo, Oct, 1965, p. Abstract No 111.
[81] P. Balk, in: Electrochem. Soc. Meet. San Fr. May, 1965, p. Abstract 109.
[82] B. E. Deal, E. L. MacKenna, and P. L. Castro, J. Electrochem. Soc. **116**, 997 (1969).
[83] W. D. Eades and R. M. Swanson, J. Appl. Phys. **58**, 4267 (1985).
[84] W. D. Eades and R. M. Swanson, J. Appl. Phys. **56**, 1744–1751 (1984).
[85] W. D. Eades and R. M. Swanson, Determination of the capture cross section and degeneracy factor of Si-SiO2 interface states, Appl. Phys. Lett. **44**, 988 (1998). http://aip.scitation.org/doi/abs/10.1063/1.94622 (accessed February 8, 2017).
[86] E. Yablonovitch, R. M. Swanson, W. D. Eades, and B. R. Weinberger, Appl. Phys. Lett. **48**, 245–247 (1986).
[87] H. Amjadi, Dielectr. Electr. Insul. IEEE Trans. **6**, 236–241 (1999).
[88] G. Declerck, R. Van Overstraeten, and G. Broux, Solid State Electron. **16**, 1451–1460 (1973).
[89] M. L. Reed and J. D. Plummer, J. Appl. Phys. **63**, 5776 (1988).
[90] K. A. Collett, R. S. Bonilla, T. C. Kho, P. Hamer, G. Bourret-Sicotte, and P. R. Wilshaw, Sol. Energy Mater. Sol. Cells (2017), in press.
[91] J. Zhao, A. Wang, and M. A. Green, Prog. Photovolt. Res. Appl. **7**, 471–474 (1999).
[92] G. Conibeer, M. Green, R. Corkish, Y. Cho, E.-C. Cho, C.-W. Jiang, T. Fangsuwannarak, E. Pink, Y. Huang, T. Puzzer, T. Trupke, B. Richards, A. Shalav, and K. Lin, Thin Solid Films **511**, 654–662 (2006).
[93] K. Lancaster, S. Großer, F. Feldmann, V. Naumann, and C. Hagendorf, Energy Procedia **92**, 116–121 (2016).
[94] F. Feldmann, M. Bivour, C. Reichel, M. Hermle, and S. W. Glunz, Sol. Energy Mater. Sol. Cells **120**, 270–274 (2014).
[95] B. L. Sopori, X. Deng, J. P. Benner, A. Rohatgi, P. Sana, S. K. Estreicher, Y. K. Park, and M. A. Roberson, Sol. Energy Mater. Sol. Cells **41–42**, 159–169 (1996).
[96] A. Beyer, M. Rennau, and G. Ebest, in: 13th Eur. Photovolt. Sol. Energy Conf., 1995, pp. 1254–1257.
[97] M. Schofthaler, R. Brendel, G. Langguth, and J. H. Werner, in: Proc. 1994 IEEE 1st World Conf. Photovolt. Energy Convers. - WCPEC (A Jt. Conf. PVSC, PVSEC PSEC), IEEE, 1994, pp. 1509–1512.
[98] J. Schmidt and A. G. Aberle, Prog. Photovolt. Res. Appl. **263**, 259–263 (1998).
[99] S. W. Glunz, D. Biro, S. Rein, and W. Warta, J. Appl. Phys. **86**, 683–691 (1999).
[100] T. C. Kho, S. C. Baker-Finch, and K. R. McIntosh, J. Appl. Phys. **109**, 53108 (2011).
[101] L. E. Black and K. R. McIntosh, IEEE Trans. Electron Dev. **57**, 1996–2004 (2010).
[102] R. S. Bonilla, C. Reichel, M. Hermle, and P. R. Wilshaw, J. Appl. Phys. **115**, 144105 (2014).
[103] R. S. Bonilla and P. R. Wilshaw, Appl. Phys. Lett. **104**, 232903 (2014).
[104] R. S. Bonilla, P. R. Wilshaw, in: Energy Procedia – Proc. 3rd Silicon PV Conf., Elsevier, Hamelin, Germany, 2013, pp. 816–822.
[105] R. S. Bonilla, C. Reichel, M. Hermle, and P. R. Wilshaw, Solid State Phenom. **205–206**, 346–351 (2013).
[106] R. S. Bonilla, C. Reichel, M. Hermle, S. Senkader, and P. R. Wilshaw, in: 2014 IEEE 40th Photovolt. Spec. Conf. (IEEE, Denver, CO, 2014), pp. 0571–0576.
[107] R. S. Bonilla, P. G. Hamer, and P. R. Wilshaw, in: EUPVSEC, Munich, Germany, 2016, pp. 707–710.
[108] R. S. Bonilla, K. Collett, L. Rands, G. Martins, R. Lobo, and P. R. Wilshaw, Solid State Phenom. **242**, 67–72 (2015).
[109] R. S. Bonilla, C. Reichel, M. Hermle, P. Hamer, and P. R. Wilshaw, Long term stability of c-Si surface passivation using corona charged SiO2, Appl. Surf. Sci. **412**, 657–667 (2017). https://doi.org/10.1016/j.apsusc.2017.03.204
[110] P. Hamer, G. Bourret-Sicotte, G. Martins, A. Wenham, R. S. Bonilla, and P. Wilshaw, A novel source of atomic hydrogen for passivation of silicon solar cells, Phys. Status Solidi RRL **11**, 1600448 (2017).
[111] G. Bourret-Sicotte, P. G. Hamer, K. A. Collett, R. S. Bonilla, and P. R. Wilshaw, Phys. Status Solidi C (2017), in press.
[112] K. R. McIntosh and X. Dai, Phys. Status Solidi **208**, 1931–1936 (2011).

[113] T. Mueller, W. Duengen, R. Job, M. Scherff, and W. Fahrner, MRS Proc. **989**, 989-A05-2 (2011).
[114] T. Mueller, S. Schwertheim, and W. R. Fahrner, J. Appl. Phys. **107**, 14504 (2010).
[115] T. Mueller, S. Schwertheim, M. Scherff, and W. R. Fahrner, Appl. Phys. Lett. **92**, 33504 (2008).
[116] T. Mueller, S. Schwertheim, and W. R. Fahrner, in: 2008 33rd IEEE Photovolatic Spec. Conf., IEEE, 2008, pp. 1–6.
[117] L. Mazzarella, S. Kolb, S. Kirner, S. Calnan, L. Korte, B. Stannowski, B. Rech, and R. Schlatmann, in: 2016 IEEE 43rd Photovolt. Spec. Conf., IEEE, 2016, pp. 2955–2959.
[118] M. Hofmann, C. Schmidt, N. Kohn, J. Rentsch, S. W. Glunz, and R. Preu, Prog. Photovolt. **16**, 509–518 (2008).
[119] P. Panek, K. Drabczyk, A. Focsa, and A. Slaoui, Mater. Sci. Eng. B **165**, 64–66 (2009).
[120] C. Leguijt, P. Lölgen, J. A. A. Eikelboom, A. W. W. Weeber, F. M. M. Schuurmans, W. C. C. Sinke, P. F. A. F. A. Alkemade, P. M. M. Sarro, C. H. M. H. M. Marée, and L. A. A. Verhoef, Sol. Energy Mater. Sol. Cells **40**, 297–345 (1996).
[121] S. Mack, A. Wolf, C. Brosinsky, S. Schmeisser, A. Kimmerle, P. Saint-Cast, M. Hofmann, and D. Biro, IEEE J. Photovolt. **1**, 135–145 (2011).
[122] F. Einsele, W. Beyer, and U. Rau, Phys. Status Solidi **7** (2010).
[123] Z. Chen, S. K. Pang, K. Yasutake, and A. Rohatgi, J. Appl. Phys. **74**, 2856–2859 (1993).
[124] G. G. Fountain, R. A. Rudder, S. V. Hattangady, R. J. Markunas, and P. S. Lindorme, J. Appl. Phys. **63**, 4744–4746 (1988).
[125] Z. Chen, K. Yasutake, A. Doolittle, and A. Rohatgi, Appl. Phys. Lett. **63**, 2117–2119 (1993).
[126] J. Ge, M. Tang, J. Wong, R. Stangl, Z. Zhang, T. Dippell, M. Doerr, O. Hohn, M. Huber, P. Wohlfart, A. G. Aberle, and T. Mueller, IEEE J. Photovolt. **5**, 705–710 (2015).
[127] J. Ge, M. Tang, J. Wong, Z. Zhang, T. Dippell, M. Doerr, O. Hohn, M. Huber, P. Wohlfart, A. G. Aberle, and T. Mueller, Int. J. Photoenergy **2014**, 1–12 (2014).
[128] G. Dingemans, C. Van Helvoirt, M. C. M. Van de Sanden, and W. M. Kessels, in: ECS Trans., The Electrochemical Society, 2011, pp. 191–204.
[129] F. L. Pasquale, S. Swaminathan, H. Kang, and A. Lavoie, ECS Trans. **53**, 147–157 (2013).
[130] H. Jung, W.-H. Kim, I.-K. Oh, C.-W. Lee, C. Lansalot-Matras, S. J. Lee, J.-M. Myoung, H.-B.-R. Lee, and H. Kim, J. Mater. Sci. **51**, 5082–5091 (2016).
[131] P. Vitanov, A. Harizanova, T. Ivanova, and H. Dikov, J. Phys. Conf. Ser. **514**, 12010 (2014).
[132] L. Huang, B. Han, B. Han, A. Derecskei-Kovacs, M. Xiao, X. Lei, M. L. O'Neill, R. M. Pearlstein, H. Chandra, and H. Cheng, J. Phys. Chem. C **117**, 19454–19463 (2013).
[133] S. Duttagupta, Advanced Surface Passivation of Crystalline Silicon for Solar Cell Applications, PhD thesis, National University of Singapore (2014).
[134] S. Duttagupta, F. J. Ma, B. Hoex, and A. G. Aberle, Sol. Energy Mater. Sol. Cells **120**, 204–208 (2014).
[135] G. Dingemans, M. C. M. van de Sanden, and W. M. M. Kessels, Phys. Status Solidi RRL **5**, 22–24 (2011).
[136] B. Hoex, F. J. J. Peeters, M. Creatore, M. A. Blauw, W. M. M. Kessels, and M. C. M. van de Sanden, J. Vac. Sci. Technol. A Vacuum Surf. Film. **24**, 1823–1830 (2006).
[137] G. Dingemans, M. M. Mandoc, S. Bordihn, M. C. M. van de Sanden, and W. M. M. Kessels, Appl. Phys. Lett. **98**, 222102 (2011).
[138] S. W. Glunz, F. Feldmann, A. Richter, M. Bivour, C. Reichel, H. Steinkemper, J. Benick, and M. Hermle, Proc. 31st Eur. Photovolt. Sol. Energy Conf. Exibition (2015), pp. 259–263.
[139] F. Feldmann, M. Bivour, C. Reichel, H. Steinkemper, M. Hermle, and S. W. Glunz, Sol. Energy Mater. Sol. Cells **131**, 46–50 (2014).
[140] N. E. Grant, K. R. McIntosh, in: 48th Annu. Conf. Aust. Sol. Energy Soc., 2010.
[141] Asuha, T. Kobayashi, O. Maida, M. Inoue, M. Takahashi, Y. Todokoro, and H. Kobayashi, Appl. Phys. Lett. **81**, 3410–3412 (2002).
[142] V. D. Mihailetchi, Y. Komatsu, and L. J. Geerligs, Appl. Phys. Lett. **92**, 63510 (2008).
[143] N. E. Grant and K. R. McIntosh, ECS J. Solid State Sci. Technol. **3**, P13–P16 (2014).
[144] N. E. Grant and K. R. McIntosh, in: 2011 37th IEEE Photovolt. Spec. Conf., IEEE, 2011, pp. 003573–003576.
[145] N. E. Grant and K. R. McIntosh, IEEE Electron Device Lett. **31**, 1002–1004 (2010).
[146] N. E. Grant and K. R. McIntosh, IEEE Electron Device Lett. **30**, 922–924 (2009).
[147] K. M. Gad, D. Vössing, P. Balamou, D. Hiller, B. Stegemann, H. Angermann, and M. Kasemann, Appl. Surf. Sci. **353**, 1269–1276 (2015).
[148] B. Stegemann, K. M. Gad, P. Balamou, D. Sixtensson, D. Vössing, M. Kasemann, and H. Angermann, Appl. Surf. Sci. **395**, 78–85 (2017).
[149] J. Cui, N. Grant, and A. Lennon, Appl. Surf. Sci. **323**, 40–44 (2014).
[150] J. Cui, X. Wang, R. Opila, and A. Lennon, J. Appl. Phys. **114**, 184101 (2013).
[151] N. E. Grant, T. C. Kho, and K. Weber, IEEE J. Photovolt. **5**, 1047–1052 (2015).
[152] A. G. Aberle, T. Lauinger, J. Schmidt, and R. Hezel, Appl. Phys. Lett. **66**, 2828 (1995).
[153] T. Lauinger, J. Schmidt, A. G. Aberle, and R. Hezel, Appl. Phys. Lett. **68**, 1232 (1996).
[154] A. G. Aberle, Sol. Energy Mater. Sol. Cells **65**, 239–248 (2001).
[155] H. Nagel, A. G. Aberle, and R. Hezel, Prog. Photovolt. Res. Appl. **7**, 245–260 (1999).
[156] T. Lauinger, J. Moschner, A. G. Aberle, and R. Hezel, J. Vac. Sci. Technol. a-Vacuum Surf. Film. **16**, 530–543 (1998).
[157] A. G. Aberle and R. Hezel, Prog. Photovoltaics Res. Appl. **5**, 29–50 (1997).
[158] R. Hezel and K. Jaeger, J. Electrochem. Soc. **136**, 518 (1989).
[159] M. J. Kerr, J. Schmidt, A. Cuevas, and J. H. Bultman, J. Appl. Phys. **89**, 3821–3826 (2001).
[160] M. J. Kerr and A. Cuevas, Semicond. Sci. Technol. **17**, 166–172 (2002).
[161] J. Schmidt, M. Kerr, and A. Cuevas, Semicond. Sci. Technol. **16**, 164–170 (2001).
[162] J. Schmidt and M. Kerr, Sol. Energy Mater. Sol. Cells **65**, 585–591 (2001).
[163] J. Schmidt and A. G. Aberle, J. Appl. Phys. **85**, 3626–3633 (1999).

[164] J. Schmidt, F. M. Schuurmans, W. C. Sinke, S. W. Glunz, and A. G. Aberle, Appl. Phys. Lett. **71**, 252 (1997).
[165] G. A. Armin, B. B. Matthew, H. Bram, and M. Thomas, GREEN **2**, 135–148 (2012).
[166] A. Goodrich, P. Hacke, Q. Wang, B. Sopori, R. Margolis, T. L. James, and M. Woodhouse, Sol. Energy Mater. Sol. Cells **114**, 110–135 (2013).
[167] Y. Wan, K. R. McIntosh, and A. F. Thomson, AIP Adv. **3**, 32113 (2013).
[168] J.-F. Lelièvre, E. Fourmond, A. Kaminski, O. Palais, D. Ballutaud, and M. Lemiti, Sol. Energy Mater. Sol. Cells **93**, 1281–1289 (2009).
[169] S. De Wolf, G. Agostinelli, G. Beaucarne, and P. Vitanov, J. Appl. Phys. **97**, 63303 (2005).
[170] S. Duttagupta, F. Lin, M. Wilson, M. B. Boreland, B. Hoex, and A. G. Aberle, Prog. Photovolt. Res. Appl. **22**, 641–647 (2014).
[171] H. Mäckel and R. Lüdemann, J. Appl. Phys. **92**, 2602 (2002).
[172] R. Hezel and R. Schörner, J. Appl. Phys. **52**, 3076–3079 (1981).
[173] W. L. Warren, F. C. Rong, E. H. Poindexter, G. J. Gerardi, and J. Kanicki, J. Appl. Phys. **70**, 346 (1991).
[174] G. H. Bauer, W. Fuhs, L. Ley, J. Kanicki, W. L. Warren, C. H. Seager, M. S. Crowder, and P. M. Lenahan, J. Non. Cryst. Solids **137**, 291–294 (1991).
[175] D. T. Krick, P. M. Lenahan, and J. Kanicki, Phys. Rev. B **38**, 8226–8229 (1988).
[176] W. L. Warren, J. Kanicki, J. Robertson, E. H. Poindexter, and P. J. McWhorter, J. Appl. Phys. **74**, 4034 (1993).
[177] A. G. Aberle, Sol. Energy Mater. Sol. Cells **65**, 239–248 (2001).
[178] W. Walukiewicz, J. Vac. Sci. Technol. B Microelectron. Nanom. Struct. **5**, 1062 (1987).
[179] F. Chen, T. Li, and J. Cotter, in: 2006 IEEE 4th World Conf. Photovolt. Energy Conf., IEEE, 2006, pp. 1020–1023.
[180] F. Chen, I. Romijn, A. Weeber, J. Tan, B. Hallam, and J. Cotter, 22nd Eiropean Photovolt. Sol. Energy Conf. Milan, Italy (2007), pp. 1053–1060.
[181] F. Chen, PECVD Silicon Nitride for N-Type Silicon Solar Cells, PhD thesis, UNSW (2008).
[182] Y. Wan, K. R. McIntosh, A. F. Thomson, and A. Cuevas, IEEE J. Photovolt. **3**, 554–559 (2013).
[183] Y. Wan, K. R. McIntosh, and A. F. Thomson, AIP Adv. **3**, 32113 (2013).
[184] Y. Wan and K. R. McIntosh, IEEE J. Photovolt. **3**, 1229–1235 (2013).
[185] W. Soppe, H. Rieffe, and A. Weeber, Prog. Photovolt. **13**, 551–569 (2005).
[186] J. D. Moschner, J. Henze, J. Schmidt, and R. Hezel, Prog. Photovolt. Res. Appl. **12**, 21–31 (2004).
[187] J. Tan, A. Cuevas, S. Winderbaum, and K. Roth, in: 20th Eur. Photovolt. Sol. Energy Conf., WIP-Renewable Energies, 2005.
[188] J. Tan, A. Cuevas, K. Hanton, S. Winderbaum, and K. Roth, Emitter Passivation and Bulk Hydrogenation Properties of Industrially Deposited Remote PECVD SiN on Si Solar Cells, in: Sol. 2004 Life, Universe Renewables, Australian and New Zealand Solar Energy Society, 2004, p. 1.
[189] S. Winderbaum, A. Cuevas, J. Tan, R. Dunn, P. Pohl, J. Schmidt, J.-L. Han, and K. Roth, in: 20th Eur. Photovolt. Sol. Energy Conf., WIP-Renewable Energies, Barcelona, Spain, 2005.
[190] S. Duttagupta, B. Hoex, and A. G. Aberle, in: 28th Eur. PVSEC, WIP, 2013, pp. 993–996.
[191] A. Wolf, S. Mack, C. Brosinsky, M. Hofmann, P. Saint-Cast, and D. Biro, in: 2011 37th IEEE Photovolt. Spec. Conf., IEEE, 2011, pp. 003568–003572.
[192] Y. Larionova, V. Mertens, N.-P. Harder, and R. Brendel, Appl. Phys. Lett. **96**, 32105 (2010).
[193] R. S. Bonilla, F. Woodcock, and P. R. Wilshaw, J. Appl. Phys. **116**, 54102 (2014).
[194] R. S. Bonilla and P. R. Wilshaw, J. Appl. Phys. **121**, 135301 (2017).
[195] Z. R. Chowdhury, K. Cho, and N. P. Kherani, Appl. Phys. Lett. **101**, 21601 (2012).
[196] A. Rohatgi, P. Doshi, J. Moschner, T. Lauinger, A. G. Aberle, and D. S. Ruby, IEEE Trans. Electron Dev. **47**, 987–993 (2000).
[197] J. Y. Lee and S. W. W. Glunz, Sol. Energy Mater. Sol. Cells **90**, 82–92 (2006).
[198] S. Narasimha and A. Rohatgi, Appl. Phys. Lett. **72**, 1872 (1998).
[199] G. Agostinelli, P. Choulat, H. F. W. Dekkers, E. Vermariën, and G. Beaucarne, in: Conf. Rec. 2006 IEEE 4th World Conf. Photovolt. Energy Conversion, WCPEC-4, IEEE, 2007, pp. 1004–1007.
[200] M. Hofmann, S. Kambor, C. Schmidt, D. Grambole, J. Rentsch, S. W. Glunz, and R. Preu, Adv. Optoelectron. **2008**, 1–10 (2008).
[201] R. Hofmann, M. Kambor, S. Schmidt, C. Grambole, D. Rentsch, J. Glunz, and S. W. Preu, in: 22nd Eur. Photovolt. Sol. Energy Conf. Exhib., 2007, p. 1030.
[202] W.-C. Cheng, J.-R. Huang, K.-Y. Yen, C.-Y. Hsieh, C.-M. Kang, S. H. T. Chen, and L.-W. Cheng, in: 2014 IEEE 40th Photovolt. Spec. Conf., IEEE, 2014, pp. 2459–2462.
[203] S. Dauwe, L. Mittelstädt, A. Metz, and R. Hezel, Prog. Photovolt. Res. Appl. **10**, 271–278 (2002).
[204] F. Gérenton, F. Mandorlo, E. Fourmond, M. Le Coz, D. Blanc-Pélissier, and M. Lemiti, J. Vac. Sci. Technol. A Vacuum Surf. Film. **34**, 51201 (2016).
[205] S. Duttagupta, Z. Hameiri, T. Grosse, D. Landgraf, B. Hoex, and A. G. Aberle, IEEE J. Photovolt. **5**, 1014–1019 (2015).
[206] S. Duttagupta, F. J. Ma, B. Hoex, and A. G. Aberle, in: Conf. Rec. IEEE Photovolt. Spec. Conf., IEEE, 2013, pp. 1776–1780.
[207] K. Wörhoff, A. Driessen, P. V. Lambeck, L. T. H. Hilderink, P. W. C. Linders, and T. J. A. Popma, Sensors Actuat. A Phys. **74**, 9–12 (1999).
[208] A. del Prado, E. San Andrés, F. L. Martínez, I. Mártil, G. González-Díaz, W. Bohne, J. Röhrich, B. Selle, and M. Fernández, Vacuum **67**, 507–512 (2002).
[209] O. P. Agnihotri, S. C. Jain, J. Poortmans, J. Szlufcik, G. Beaucarne, J. Nijs, and R. Mertens, Semicond. Sci. Technol. **15**, R29–R40 (2000).
[210] M. Lipiński, A. Kaminski, J.-F. Lelièvre, M. Lemiti, E. Fourmond, and P. Zięba, Phys. Status Solidi **4**, 1566–1569 (2007).
[211] J. Dupuis, E. Fourmond, J. F. Lelièvre, D. Ballutaud, and M. Lemiti, Thin Solid Films **516**, 6954–6958 (2008).
[212] J. Dupuis, E. Fourmond, V. M.-T. Yen, O. Nichiporuk, M. Greffioz, N. Le Quang, and M. Lemiti, in: 24th Eur.

Photovolt. Sol. Energy Conf., Hamburg, Germany, 2009, pp. 1623–1627.
[213] J. Dupuis, E. Fourmond, D. Ballutaud, N. Bererd, and M. Lemiti, Thin Solid Films **519**, 1325–1333 (2010).
[214] J. Seiffe, L. Gautero, M. Hofmann, J. Rentsch, R. Preu, S. Weber, and R. A. Eichel, J. Appl. Phys. **109**, 34105 (2011).
[215] J. Rentsch, L. Gautero, M. Hofmann, L. Weiss, and J. Seiffe, 23rd Eur. Photovolt. Sol. Energy Conf. Exhib. 1–5 Sept. 2008, Val. Spain (2008), pp. 1700–1703.
[216] A. Lawerenz, H. Strutzberg, C. Leschinski, M. Roczen, C. Maier, H. C. Biank, M. Blech, and A. Laades, 26th Eur. Photovolt. Sol. Energy Conf. Exhib. (2011), pp. 1653–1658.
[217] C. Schwab, M. Hofmann, R. Heller, J. Seiffe, J. Rentsch, and R. Preu, Phys. Status Solidi **210**, 2399–2403 (2013).
[218] C. Zhou, J. Zhu, S. E. Foss, H. Haug, Ø. Nordseth, E. S. Marstein, and W. Wang, Energy Procedia **77**, 434–439 (2015).
[219] C. Zhou, J. Zhu, S. Zhou, Y. Tang, S. E. Foss, H. Haug, Ø. Nordseth, E. S. Marstein, and W. Wang, Prog. Photovolt. Res. Appl. **25**, 23–32 (2016).
[220] N. Brinkmann, D. Sommer, G. Micard, G. Hahn, and B. Terheiden, Sol. Energy Mater. Sol. Cells **108**, 180–188 (2013).
[221] V. Naumann, D. Lausch, A. Hähnel, J. Bauer, O. Breitenstein, A. Graff, M. Werner, S. Swatek, S. Großer, J. Bagdahn, and C. Hagendorf, Sol. Energy Mater. Sol. Cells **120**, 383–389 (2014).
[222] S. Pingel, O. Frank, M. Winkler, S. Daryan, T. Geipel, H. Hoehne, and J. Berghold, in: 2010 35th IEEE Photovolt. Spec. Conf., IEEE, 2010, pp. 002817–002822.
[223] J. Zhu, S. Zhou, H. Haug, E. S. Stensrud Marstein, S. E. Foss, and W. Wang, 29th Eur. Photovolt. Sol. Energy Conf. Exhib. (2014), pp. 1100–1103.
[224] X. Cheng, H. Haug, M. Di Sabatino, J. Zhu, and E. S. Marstein, IEEE J. Photovolt. **6**, 1103–1108 (2016).
[225] B. Hallam, B. Tjahjono, and S. Wenham, Sol. Energy Mater. Sol. Cells **96**, 173–179 (2012).
[226] Z. Zhuo, Y. Sannomiya, Y. Kanetani, T. Yamada, H. Ohmi, H. Kakiuchi, and K. Yasutake, Nanoscale Res. Lett. **8**, 201 (2013).
[227] B. Hoex, A. J. M. van Erven, R. C. M. Bosch, W. T. M. Stals, M. D. Bijker, P. J. van den Oever, W. M. M. Kessels, and M. C. M. van de Sanden, Prog. Photovolt. Res. Appl. **13**, 705–712 (2005).
[228] M. Vetter, Thin Solid Films **337**, 118–122 (1999).
[229] P. M. Kaminski, K. Bass, G. Claudio, and J. M. Walls, Appl. Surf. Sci. **301**, 51–55 (2014).
[230] P. Fath, S. Keller, P. Winter, T. Frieß, H. Habenicht, K. Varner, A. Yodyunyong, R. E. Schlosser, J. Maier, A. Teppe, M. Hein, M. Hanke, J. Schöne, and K. A. Münzer, 27th Eur. Photovolt. Sol. Energy Conf. Exhib. (2012), pp. 666–671.
[231] H. Yang, E. Wang, H. Wang, and W. Guo, Energy Procedia **88**, 389–393 (2016).
[232] M. Tanaka, M. Taguchi, T. Matsuyama, T. Sawada, S. Tsuda, S. Nakano, H. Hanafusa, and Y. Kuwano, Jpn. J. Appl. Phys. **31**, 3518–3522 (1992).
[233] T. Mishima, M. Taguchi, H. Sakata, and E. Maruyama, Sol. Energy Mater. Sol. Cells **95**, 18–21 (2011).
[234] W. G. J. H. M. van Sark, L. Korte, and F. Roca, eds., Physics and Technology of Amorphous-Crystalline Heterostructure Silicon Solar Cells (Springer Berlin Heidelberg, Berlin, Heidelberg, 2012).
[235] T. Sawada, N. Terada, S. Tsuge, T. Baba, T. Takahama, K. Wakisaka, S. Tsuda, and S. Nakano, in:, Proc. 1994 IEEE 1st World Conf. Photovolt. Energy Convers. – WCPEC (A Jt. Conf. PVSC, PVSEC PSEC), IEEE, n.d., pp. 1219–1226.
[236] H. Matsuura, T. Okuno, H. Okushi, and K. Tanaka, J. Appl. Phys. **55**, 1012–1019 (1984).
[237] S. De Wolf, A. Descoeudres, Z. C. Holman, and C. Ballif, Green **2**, 7–24 (2012).
[238] J. Geissbühler, J. Werner, S. M. De Nicolas, L. Barraud, A. Hessler-Wyser, M. Despeisse, S. Nicolay, A. Tomasi, B. Niesen, S. De Wolf, and C. Ballif, Appl. Phys. Lett. **1071**, 81601 (2015).
[239] S. Muramatsu, T. Uematsu, Y. Nagata, H. Ohtsuka, and T. Warabisako, Sol. Energy Mater. Sol. Cells **48**, 151–157 (1997).
[240] M. W. M. van Cleef, F. M. Schuurmans, A. S. H. van der Heide, A. Schönecker, and R. E. I. Schropp, Passivation of c-Si solar cells by low temperature H-treatments and deposited a-Si:H layers, in: 2nd World Conf. Photovolt. Sol. Energy Convers., 1998: pp. 1661–1664.
[241] M. Taguchi, K. Kawamoto, S. Tsuge, T. Baba, H. Sakata, M. Morizane, K. Uchihashi, N. Nakamura, S. Kiyama, and O. Oota, Prog. Photovolt. Res. Appl. **8**, 503–513 (2000).
[242] E. Centurioni, D. Iencinella, R. Rizzoli, and F. Zignani, IEEE Trans. Electron Dev. **51**, 1818–1824 (2004).
[243] S. Dauwe, Low-Temperature Surface Passivation of Crystalline Silicon and its Application to the Rear Side of Solar Cells, PhD thesis, Univeristy of Hannover (2004).
[244] S. Dauwe, J. Schmidt, and R. Hezel, in: 29th IEEE Photovolt. Spec. Conf., 2002, p. 1246.
[245] S. Dauwe, L. Mittelstadt, A. Metz, J. Schmidt, and R. Hezel, in: 3rd World Conf. Photovolt. Energy Convers., 2003, p. 1395.
[246] S. De Wolf and M. Kondo, Appl. Phys. Lett. **90**, 42111 (2007).
[247] S. De Wolf, C. Ballif, and M. Kondo, Phys. Rev. B – Condens. Matter Mater. Phys. **85**, 113302 (2012).
[248] M. Z. Burrows, U. K. Das, R. L. Opila, S. De Wolf, and R. W. Birkmire, J. Vac. Sci. Technol. A Vacuum Surf. Film. **26**, 683 (2008).
[249] S. Olibet, E. Vallat-Sauvain, L. Fesquet, C. Monachon, A. Hessler-Wyser, J. Damon-Lacoste, S. De Wolf, and C. Ballif, Phys. Status Solidi **207**, 651–656 (2010).
[250] S. Olibet, E. Vallat-Sauvain, and C. Ballif, Phys. Rev. B **76**, 35326 (2007).
[251] A. Descoeudres, L. Barraud, R. Bartlome, G. Choong, S. De Wolf, F. Zicarelli, and C. Ballif, Appl. Phys. Lett. **97**, 183505 (2010).
[252] S. De Wolf, B. Demaurex, A. Descoeudres, and C. Ballif, Phys. Rev. B **83**, 233301 (2011).
[253] S. De Wolf and M. Kondo, J. Appl. Phys. **105**, 103707 (2009).
[254] S. De Wolf, S. Olibet, and C. Ballif, Appl. Phys. Lett. **93**, 32101 (2008).
[255] A. Descoeudres, L. Barraud, S. De Wolf, B. Strahm, D. Lachenal, C. Guérin, Z. C. Holman, F. Zicarelli, B. Demaurex, J. Seif, J. Holovsky, and C. Ballif, Appl. Phys. Lett. **99**, 123506 (2011).
[256] J.-W. A. Schüttauf, K. H. M. van der Werf, I. M. Kielen, W. G. J. H. M. van Sark, J. K. Rath, and R. E. I. Schropp, Appl. Phys. Lett. **98**, 153514 (2011).

[257] B. Strahm, Y. Andrault, D. Baetzner, C. Guérin, N. Holmes, M. Kobas, D. Lachenal, B. Mendes, M. Tesfai, G. Wahli, F. Wuensch, A. Buechel, J. Mai, T. Schulze, and M. Vogt, in: 25th Eur. Photovolt. Sol. Energy Conf. Exhib./5th World Conf. Photovolt. Energy Conversion, 6–10 Sept. 2010, Val. Spain, WIP-Munich, 2010, pp. 1286–1289.
[258] J. Peter Seif, A. Descoeudres, M. Filipič, F. Smole, M. Topič, Z. Charles Holman, S. De Wolf, and C. Ballif, J. Appl. Phys. **115**, 24502 (2014).
[259] M. Mews, M. Liebhaber, B. Rech, and L. Korte, Appl. Phys. Lett. **107**, 13902 (2015).
[260] B. Stegemann, J. Kegel, M. Mews, E. Conrad, L. Korte, U. Stürzebecher, and H. Angermann, Energy Procedia **38**, 881–889 (2013).
[261] D. Muñoz, P. Carreras, J. Escarré, D. Ibarz, S. Martín de Nicolás, C. Voz, J. M. Asensi, and J. Bertomeu, Thin Solid Films **517**, 3578–3580 (2009).
[262] H. Angermann, E. Conrad, L. Korte, J. Rappich, T. F. Schulze, and M. Schmidt, Mater. Sci. Eng. B **159**, 219–223 (2009).
[263] A. Descoeudres, Z. C. Holman, L. Barraud, S. Morel, S. De Wolf, and C. Ballif, IEEE J. Photovolt. **3**, 83–89 (2013).
[264] Y. Wan, D. Yan, J. Bullock, X. Zhang, and A. Cuevas, Appl. Phys. Lett. **107**, 231606 (2015).
[265] S. Y. Herasimenka, C. J. Tracy, V. Sharma, N. Vulic, W. J. Dauksher, and S. G. Bowden, Appl. Phys. Lett. **103**, 183903 (2013).
[266] R. S. Bonilla, C. Reichel, M. Hermle, and P. R. Wilshaw, Extremely low surface recombination in 1 Ω cm n-type monocrystalline silicon, Phys. Status Solidi RRL **11**, 1600307 (2016). https://doi.org/10.1002/pssr.2016 00307
[267] K. Nakada, S. Miyajima, and M. Konagai, Jpn. J. Appl. Phys. **53**, 04ER13 (2014).
[268] S. Gerke, H.-W. Becker, D. Rogalla, G. Hahn, R. Job, and B. Terheiden, Energy Procedia **77**, 791–798 (2015).
[269] H. Li, B. Hallam, and S. R. Wenham, in: 2011 37th IEEE Photovolt. Spec. Conf., IEEE, 2011, pp. 001481–001485.
[270] S. Bowden, U. Das, S. Herasimenka, and R. Birkmire, in: 2008 33rd IEEE Photovolatic Spec. Conf., IEEE, 2008, pp. 1–4.
[271] A. G. Ulyashin, A. Bentzen, S. Diplas, A. Suphellen, A. E. Gunnaes, A. Olsen, B. G. Svensson, E. S. Marstein, A. Holt, D. Grambole, and E. Sauar, in: 2006 IEEE 4th World Conf. Photovolt. Energy Conf., IEEE, 2006, pp. 1354–1357.
[272] S. Gatz, H. Plagwitz, P. P. Altermatt, B. Terheiden, and R. Brendel, 23rd Eur. Photovolt. Sol. Energy Conf. Exhib. (2008), p. 1033.
[273] Y. Wan, D. Yan, J. Bullock, X. Zhang, and A. Cuevas, Appl. Phys. Lett. **107**, 231606 (2015).
[274] B. Hekmatshoar, D. Shahrjerdi, M. Hopstaken, and D. Sadana, in: 2011 Int. Reliab. Phys. Symp., IEEE, 2011, pp. 5E.5.1–5E.5.4.
[275] H. Angermann, F. Wünsch, M. Kunst, A. Laades, U. Stürzebecher, E. Conrad, L. Korte, and M. Schmidt, Phys. Status Solidi **8**, 879–882 (2011).
[276] B. Hoex, F. J. J. Peeters, A. j. Erven, M. D. Bijker, W. M. M. Kessels, and M. c. m. De Sanden, in: 2006 IEEE 4th World Conf. Photovolt. Energy Conf., IEEE, 2006, pp. 1036–1039.
[277] B. Halliop, M. F. Salaun, W. Favre, R. Varache, M. E. Gueunier-Farret, J. P. Kleider, and N. P. Kherani, J. Non. Cryst. Solids **358**, 2227–2231 (2012).
[278] S. Gerke, G. Hahn, R. Job, and B. Terheiden, Energy Procedia **84**, 105–109 (2015).
[279] J.-W. A. Schuttauf, K. H. M. van der Werf, I. M. Kielen, W. G. J. H. M. van Sark, J. K. Rath, and R. E. I. Schropp, Appl. Phys. Lett. **99**, 203503 (2011).
[280] D. Y. Jeong, K. Kim, H. Song, J. Song, S. J. Baik, and J. C. Lee, Renew. Energy **68**, 397–402 (2014).
[281] K. Koyama, K. Ohdaira, and H. Matsumura, Appl. Phys. Lett. **97**, 82108 (2010).
[282] M. Schaper, J. Schmidt, H. Plagwitz, and R. Brendel, Prog. Photovolt. Res. Appl. **13**, 381–386 (2005).
[283] M. Filipi, Z. C. Holman, F. Smole, S. De Wolf, C. Ballif, and M. Topi, J. Appl. Phys. **114**, 74504 (2013).
[284] T. Dullweber and J. Schmidt, IEEE J. Photovolt. **6**, 1366–1381 (2016).
[285] M. Hofmann, S. Glunz, R. Preu, and G. Willeke, in: 21st Eur. Photovolt. Sol. Energy Conf., 2006, pp. 609–612.
[286] K. Carstens, M. Dahlinger, E. Hoffmann, J. R. Köhler, R. Zapf-Gottwick, and J. H. Werner, Energy Procedia **77**, 779–785 (2015).
[287] Z. Shu, U. Das, J. Allen, R. Birkmire, and S. Hegedus, Prog. Photovolt. Res. Appl. **23**, 78–93 (2015).
[288] K. Jäger and R. Hezel, in: Proc. 18th IEEE PVSC, 1985, p. 1752.
[289] D. König and G. Ebest, Solid. State. Electron. **44**, 111–116 (2000).
[290] D. König, M. Rennau, M. Henker, and G. Ebest, Thin Solid Films **385**, 126–131 (2001).
[291] G. B. G Agostinelli, P Vitanov, Z Alexieva, A Harizanova, H. F. W Dekkers, and S. De Wolf, in: Proc. 19th Eur. Photovolt. Sol. Energy Conf. Paris, Fr., 2004, pp. 132–134.
[292] G. Agostinelli, A. Delabie, P. Vitanov, Z. Alexieva, H. F. W. F. W. Dekkers, S. De Wolf, and G. Beaucarne, Sol. Energy Mater. Sol. Cells **90**, 3438–3443 (2006).
[293] B. Hoex, S. B. S. Heil, E. Langereis, M. C. M. van de Sanden, and W. M. M. Kessels, Appl. Phys. Lett. **89**, 42112 (2006).
[294] B. Hoex, J. J. H. Gielis, M. C. M. van de Sanden, and W. M. M. Kessels, J. Appl. Phys. **104**, 113703 (2008).
[295] B. Hoex, J. Schmidt, P. Pohl, M. C. M. van de Sanden, and W. M. M. Kessels, J. Appl. Phys. **104**, 44903 (2008).
[296] P. Saint-Cast, D. Kania, M. Hofmann, J. Benick, J. Rentsch, and R. Preu, Appl. Phys. Lett. **95**, 151502 (2009).
[297] J. Schmidt, A. Merkle, R. Brendel, B. Hoex, M. C. M. Van De Sanden, and W. M. M. Kessels, Prog. Photovolt. Res. Appl. **16**, 461–466 (2008).
[298] J. Benick, B. Hoex, M. C. M. Van De Sanden, W. M. M. Kessels, O. Schultz, and S. W. Glunz, Appl. Phys. Lett. **92**, 253504 (2008).
[299] S. Duttagupta, F.-J. Ma, S. F. Lin, T. Mueller, A. G. Aberle, and B. Hoex, IEEE J. Photovolt. **3**, 1163–1169 (2013).
[300] A. Richter, J. Benick, M. Hermle, and S. W. Glunz, Phys. Status Solidi – Rapid Res. Lett. **5**, 202–204 (2011).
[301] A. Richter, J. Benick, and M. Hermle, IEEE J. Photovolt. **3**, 236–245 (2013).
[302] A. Richter, J. Benick, A. Kalio, J. Seiffe, M. Hörteis, M. Hermle, and S. W. Glunz, Energy Procedia **8**, 479–486 (2011).
[303] J. Benick, A. Richter, T.-T. A. Li, N. E. Grant, K. R. McIntosh, Y. Ren, K. J. Weber, M. Hermle, and S. W.

Glunz, in: 2010 35th IEEE Photovolt. Spec. Conf., IEEE, 2010, pp. 000891–000896.
[304] A. Richter, M. Hoteis, J. Benick, S. Henneck, M. Hermle, and S. W. Glunz, in: 2010 35th IEEE Photovolt. Spec. Conf., IEEE, 2010, pp. 003587–003592.
[305] A. Richter, J. Benick, M. Hermle, and S. W. Glunz, Appl. Phys. Lett. **104**, 61606 (2014).
[306] J. Benick, A. Richter, M. Hermle, and S. W. Glunz, Phys. Status Solidi RRL **3**, 233–235 (2009).
[307] G. Dingemans, N. M. Terlinden, D. Pierreux, H. B. Profijt, M. C. M. van de Sanden, W. M. M. M. Kessels, M. C. M. van de Sanden, and W. M. M. M. Kessels, Electrochem. Solid-State Lett. **14**, H1–H4 (2011).
[308] G. Dingemans, N. M. Terlinden, M. A. Verheijen, M. C. M. van de Sanden, and W. M. M. Kessels, J. Appl. Phys. **110**, 093715 (2011).
[309] G. Dingemans and E. Kessels, J. Vac. Sci. Technol. A **30**, 1–27 (2012).
[310] G. Dingemans, R. Seguin, P. Engelhart, M. C. M. van den Sanden, and W. M. M. Kessels, Phys. Status Solidi RRL **4**(1–2), 10–12 (2010).
[311] G. Dingemans, W. Beyer, M. C. M. van de Sanden, and W. M. M. Kessels, Appl. Phys. Lett. **97**, 152106 (2010).
[312] N. M. Terlinden, G. Dingemans, M. C. M. van de Sanden, and W. M. M. Kessels, Appl. Phys. Lett. **96**, 112101 (2010).
[313] G. Dingemans, P. Engelhart, R. Seguin, F. Einsele, B. Hoex, M. C. M. van de Sanden, and W. M. M. Kessels, J. Appl. Phys. **106**, 114907 (2009).
[314] G. Dingemans, M. C. M. van de Sanden, and W. M. M. Kessels, Plasma Process. Polym. **9**, 761–771 (2012).
[315] P. Saint-cast, Passivation of Si Surfaces by PECVD Aluminum Oxide (University of Konstanz, PhD Thesis, 2012).
[316] P. Saint-Cast, A. Richter, E. Billot, M. Hofmann, J. Benick, J. Rentsch, R. Preu, and S. W. Glunz, Thin Solid Films **522**, 336–339 (2012).
[317] P. Saint-Cast, Y.-H. Heo, E. Billot, P. Olwal, M. Hofmann, J. Rentsch, S. W. Glunz, and R. Preu, Energy Procedia **8**, 642–647 (2011).
[318] P. Saint-Cast, D. Kania, R. Heller, S. Kuehnhold, M. Hofmann, J. Rentsch, and R. Preu, Appl. Surf. Sci. **258**, 8371–8376 (2012).
[319] G. Dingemans, R. Seguin, P. Engelhart, M. C. M. van de Sanden, and W. M. M. Kessels, Phys. Status Solidi – Rapid Res. Lett. **4**, 10–12 (2010).
[320] H. B. Profijt, S. E. Potts, M. C. M. van de Sanden, and W. M. M. Kessels, J. Vac. Sci. Technol. A **29**, 50801 (2011).
[321] G. G. Untila, T. N. Kost, A. B. Chebotareva, M. B. Zaks, A. M. Sitnikov, and O. I. Solodukha, Semiconductors **46**, 832–837 (2012).
[322] S. Kühnhold-Pospischil, P. Saint-Cast, A. Richter, and M. Hofmann, Appl. Phys. Lett. **109**, 61602 (2016).
[323] H. B. Profijt, P. Kudlacek, M. C. M. van de Sanden, and W. M. M. Kessels, J. Electrochem. Soc. **158**, G88 (2011).
[324] B. Veith, T. Dullweber, M. Siebert, C. Kranz, F. Werner, N. P. Harder, J. Schmidt, B. F. P. Roos, T. Dippell, and R. Brendel, Energy Procedia **27**, 379–384 (2012).
[325] V. Verlaan, L. R. J. G. Van Den Elzen, G. Dingemans, M. C. M. Van De Sanden, and W. M. M. Kessels, Phys. Status Solidi C **7**, 976–979 (2010).
[326] D. Hoogeland, K. B. Jinesh, F. Roozeboom, W. F. A. Besling, M. C. M. van de Sanden, and W. M. M. Kessels, J. Appl. Phys. **106**, 114107 (2009).
[327] R. S. Johnson, G. Lucovsky, and I. Baumvol, J. Vac. Sci. Technol. A **19**, 1353–1360 (2001).
[328] E. Simoen, A. Rothschild, B. Vermang, J. Poortmans, and R. Mertens, Electrochem. Solid-State Lett. **14**, H362 (2011).
[329] A. Stesmans and V. V. Afanas'ev, Appl. Phys. Lett. **80**, 1957–1959 (2002).
[330] S. Baldovino, S. Nokhrin, G. Scarel, M. Fanciulli, T. Graf, and M. S. Brandt, J. Non. Cryst. Solids **322**, 168–173 (2003).
[331] B. Liao, R. Stangl, F. Ma, T. Mueller, F. Lin, A. G. Aberle, C. S. Bhatia, and B. Hoex, J. Phys. D. Appl. Phys. **46**, 385102 (2013).
[332] P. Poodt, D. C. Cameron, E. Dickey, S. M. George, V. Kuznetsov, G. N. Parsons, F. Roozeboom, G. Sundaram, and A. Vermeer, J. Vac. Sci. Technol. A **30**, 10802 (2012).
[333] W. M. M. (Erwin) Kessels and M. Putkonen, MRS Bull. **36**, 907–913 (2011).
[334] B. Hoex, Futur. PV **7**, 1–7 (2012).
[335] A. Richter, F. M. M. Souren, D. Schuldis, R. M. W. Görtzen, J. Benick, M. Hermle, and S. W. Glunz, in: 27th Eur. Photovolt. Sol. Energy Conf. Exhib. Frankfurt, Germany, WIP, 2012, pp. 1133–1137.
[336] S. Miyajima, J. Irikawa, A. Yamada, and M. Konagai, Appl. Phys. Express **3**, 12301 (2010).
[337] S. Bordihn, J. A. Van Delft, M. M. Mandoc, J. W. Müller, and W. M. M. Kessels, IEEE J. Photovolt. **3**, 970–975 (2013).
[338] D. Schuldis, A. Richter, J. Benick, P. Saint-Cast, M. Hermle, and S. W. Glunz, Appl. Phys. Lett. **105**, 231601 (2014).
[339] J. Schmidt, B. Veith, and R. Brendel, Phys. Status Solidi RRL **3**, 287–289 (2009).
[340] G. Dingemans, F. Einsele, W. Beyer, M. C. M. Van de Sanden, and W. M. M. Kessels, J. Appl. Phys. **111**, 93713 (2012).
[341] J. A. Töfflinger, A. Laades, L. Korte, C. Leendertz, L. M. Montañez, U. Stürzebecher, H.-P. Sperlich, and B. Rech, Sol. Energy Mater. Sol. Cells **135**, 49–56 (2015).
[342] G. Dingemans, N. M. Terlinden, M. A. Verheijen, M. C. M. Van De Sanden, and W. M. M. Kessels, J. Appl. Phys. **110**, 93715 (2011).
[343] B. W. H. van de Loo, H. C. M. Knoops, G. Dingemans, G. J. M. Janssen, M. W. P. E. Lamers, I. G. Romijn, A. W. Weeber, and W. M. M. Kessels, Sol. Energy Mater. Sol. Cells **143**, 450–456 (2015).
[344] L. E. Black, New Perspectives on Surface Passivation: Understanding the Si-Al2O3 Interface (Springer International Publishing, Cham, 2016).
[345] L. E. Black, T. Allen, A. Cuevas, K. R. McIntosh, B. Veith, and J. Schmidt, Sol. Energy Mater. Sol. Cells **120**, 339–345 (2014).
[346] L. E. Black, T. Allen, K. R. McIntosh, and A. Cuévas, Energy Procedia **92**, 317–325 (2016).
[347] K. Kern and E. Tracy, RCA Rev. (United States) **41** (1980).
[348] M. Murozono, S. Kitamura, T. Ohmura, K. Kusao, and Y. Umeo, Jpn. J. Appl. Phys. **21**, 137 (1982).
[349] D. C. Wong and A. Waugh, MRS Proc. **426**, 503 (1996).
[350] J. Szlufcik, J. Majewski, A. Buczkowski, J. Radojewski, L. Jędral, and E. B. Radojewska, Sol. Energy Mater. **18**, 241–252 (1989).

[351] K. O. Davis, K. Jiang, D. Habermann, and W. V. Schoenfeld, IEEE J. Photovolt. **5**, 1265–1270 (2015).
[352] B. S. Richards, Sol. Energy Mater. Sol. Cells **79**, 369–390 (2003).
[353] `T. Watanabe, A. Nakajima, R. Wang, M. Minabe, S. Koizumi, A. Fujishima, and K. Hashimoto, Thin Solid Films **351**, 260–263 (1999).
[354] S. A. O'Neill, I. P. Parkin, R. J. H. Clark, A. Mills, and N. Elliott, J. Mater. Chem. **13**, 56–60 (2003).
[355] B. S. Richards, Prog. Photovolt. Res. Appl. **12**, 253–281 (2004).
[356] A. F. Thomson and K. R. McIntosh, Prog. Photovolt. Res. Appl. **20**, 343–349 (2012).
[357] B. Liao, B. Hoex, A. G. Aberle, D. Chi, and C. S. Bhatia, Appl. Phys. Lett. **104**, 253903 (2014).
[358] B. Liao, B. Hoex, K. D. Shetty, P. K. Basu, and C. S. Bhatia, IEEE J. Photovolt. **5**, 1062–1066 (2015).
[359] J. Cui, T. Allen, Y. Wan, J. Mckeon, C. Samundsett, D. Yan, X. Zhang, Y. Cui, Y. Chen, P. Verlinden, and A. Cuevas, Sol. Energy Mater. Sol. Cells **158**, 115–121 (2016).
[360] R. S. Bonilla, K. Davis, E. Schneller, G. Bourret-Sicotte, P. Hame, W. V. Schoenfeld, and P. R. Wilshaw, Effective antireflection and surface passivation of silicon using a SiO2/a-TiOx film stack, Submiss. to IEEE J. Photovoltaics. (2017).
[361] M. Vetter, R. Ferre, I. Martin, P. Ortega, R. Alcubilla, R. Petres, J. Libal, and R. Kopecek, in: Conf. Rec. 2006 IEEE 4th World Conf. Photovolt. Energy Conversion, WCPEC-4, IEEE, 2007, pp. 1271–1274.
[362] R. Ferre, A. Orpella, D. Munoz, I. Martín, F. Recart, C. Voz, J. Puigdollers, P. R. i Cabarrocas, and R. Alcubilla, Prog. Photovolt. Res. Appl. **16**, 123–127 (2008).
[363] I. Martín, M. Vetter, A. Orpella, J. Puigdollers, A. Cuevas, and R. Alcubilla, Appl. Phys. Lett. **79**, 2199–2201 (2001).
[364] A. Orpella, S. Blanque, V. Roiati, I. Martin, C. Voz, J. Puigdollers, and R. Alcubilla, in: 2009 Spanish Conf. Electron Devices, IEEE, 2009, pp. 357–359.
[365] I. Martín, M. Vetter, A. Orpella, C. Voz, J. Puigdollers, and R. Alcubilla, Appl. Phys. Lett. **81**, 4461–4463 (2002).
[366] S. Janz, S. Riepe, M. Hofmann, S. Reber, and S. Glunz, Appl. Phys. Lett. **88**, 133516 (2006).
[367] S. Kerdiles, R. Madelon, and R. Rizk, Appl. Surf. Sci. **184**, 150–155 (2001).
[368] Y. Xie, L. Cheng, H. Mei, and L. Zhang, J. Compos. Mater. **49**, 2441–2447 (2015).
[369] E. Chen, G. Du, Y. Zhang, X. Qin, H. Lai, and W. Shi, Ceram. Int. **40**, 9791–9797 (2014).
[370] M. Boccard, A. Jackson, and Z. C. Holman, 2016 IEEE 43rd Photovolt. Spec. Conf. (2016), pp. 5–7.
[371] M. Boccard and Z. C. Holman, J. Appl. Phys. **118**, 65704 (2015).
[372] D. Suwito, T. Roth, D. Pysch, L. Korte, A. Richter, S. Janz, and S. W. Glunz, in: 23rd Eur. Photovolt. Sol. Energy Conf. Exhibition, 1–5 Sept. 2008, Val. Spain, WIP-Munich, 2008, pp. 1023–1028.
[373] P. M. Kaminski, A. Abbas, K. Bass, and G. Claudio, Energy Procedia **10**, 71–75 (2011).
[374] Y.-H. Joung, F.-S. Kang, H. Il Kang, W. S. Choi, and J. Yoo, Thin Solid Films **587**, 160–162 (2015).
[375] M. H. Kang, A. Ebong, B. Rounsaville, A. Rohatgi, and J. Hong, in: 2009 34th IEEE Photovolt. Spec. Conf., IEEE, 2009, pp. 001724–001726.
[376] M. H. Kang, D. S. Kim, A. Ebong, B. Rounsaville, A. Rohatgi, G. Okoniewska, and J. Hong, J. Electrochem. Soc. **156**, H495–H499 (2009).
[377] I. Martín, P. Ortega, M. Colina, A. Orpella, G. López, and R. Alcubilla, Prog. Photovolt. Res. Appl. **21**, n/a-n/a (2012).
[378] U. Coscia, G. Ambrosone, P. Rava, P. Rivolo, F. Ferrazza, L. Serenelli, S. De Iuliis, and M. Tucci, Thin Solid Films **516**, 1569–1573 (2008).
[379] S. Glunz, S. Janz, M. Hofmann, T. Roth, and G. Willeke, in: 2006 IEEE 4th World Conf. Photovolt. Energy Conf., IEEE, 2006, pp. 1016–1019.
[380] F. Lin, B. Hoex, Y. H. Koh, J. J. Lin, and A. G. Aberle, Energy Procedia **15**, 84–90 (2012).
[381] F. Lin, B. Hoex, Y. H. Koh, J. Lin, A. G. Aberle, E. C. S. J. Solid, S. Sci, and P. N-n, ECS J. Solid State Sci. Technol. **2**, 1–5 (2013).
[382] J. Wang, S. Sadegh Mottaghian, and M. Farrokh Baroughi, IEEE Trans. Electron Dev. **59**, 342–348 (2012).
[383] R. Sreenivasan, P. C. McIntyre, H. Kim, and K. C. Saraswat, Appl. Phys. Lett. **89**, 112903 (2006).
[384] J. Gope, Vandana, N. Batra, J. Panigrahi, R. Singh, K. K. Maurya, R. Srivastava, and P. K. Singh, Appl. Surf. Sci. **357**, 635–642 (2015).
[385] G. Dingemans and W. M. M. Kessels, in: ECS Trans., The Electrochemical Society, 2011, pp. 293–301.
[386] X. Cheng, P. Repo, H. Halvard, A. P. Perros, E. S. Marstein, M. Di Sabatino, and H. Savin, IEEE J. Photovolt. **7**, 479–485 (2017).
[387] J. Cui, Y. Wan, Y. Cui, Y. Chen, P. Verlinden, and A. Cuevas, Appl. Phys. Lett. **110**, 21602 (2017).
[388] T. G. Allen and A. Cuevas, Appl. Phys. Lett. **105**, 31601 (2014).
[389] T. G. Allen and A. Cuevas, Phys. Status Solidi RRL **9**, 220–224 (2015).
[390] T. G. Allen, Y. Y. Wan, and A. Cuevas, IEEE J. Photovolt. **6**, 900–905 (2016).
[391] T. G. Allen, M. Ernst, C. Samundsett, and A. Cuevas, in: 2015 IEEE 42nd Photovolt. Spec. Conf., IEEE, 2015, pp. 1–6.
[392] Y. Wan, J. Bullock, and A. Cuevas, Appl. Phys. Lett. **106**, 201601 (2015).
[393] Y. Wan, J. Bullock, and A. Cuevas, Sol. Energy Mater. Sol. Cells **142**, 42–46 (2015).
[394] P. Repo, Y. Bao, H. Seppanen, P. Sippola, and H. Savin, in: 2016 IEEE 43rd Photovolt. Spec. Conf., IEEE, 2016, pp. 2967–2970.
[395] R. S. Bonilla, N. Jennison, D. Clayton-Warwick, K. A. Collett, L. Rands, and P. R. Wilshaw, Energy Procedia **92**, 326–335 (2016).
[396] D. Yan, A. Cuevas, Y. Wan, and J. Bullock, Sol. Energy Mater. Sol. Cells **152**, 73–79 (2016).
[397] Y. Wan, C. Samundsett, D. Yan, T. Allen, J. Peng, J. Cui, X. Zhang, J. Bullock, and A. Cuevas, Appl. Phys. Lett. **109**, 113901 (2016).
[398] Y. Wan, C. Samundsett, J. Bullock, M. Hettick, T. Allen, D. Yan, J. Peng, Y. Wu, J. Cui, A. Javey, and A. Cuevas, Adv. Energy Mater. **7**, 1601863 (2016).
[399] T. G. Allen, J. Bullock, Q. Jeangros, C. Samundsett, Y. Wan, J. Cui, A. Hessler-Wyser, S. De Wolf, A. Javey, and A. Cuevas, Adv. Energy Mater. 1602606 (2017).
[400] J. Bullock, Y. Wan, M. Hettick, J. Geissbuhler, A. J. Ong, D. Kiriya, D. Yan, T. Allen, J. Peng, X. Zhang, C. M. Sutter-Fella, S. De Wolf, C. Ballif, A. Cuevas, and A. Javey, in:

2016 IEEE 43rd Photovolt. Spec. Conf., IEEE, 2016, pp. 0210–0214.
[401] C. Reichel, F. Feldmann, R. Müller, R. C. Reedy, B. G. Lee, D. L. Young, P. Stradins, M. Hermle, and S. W. Glunz, J. Appl. Phys. **118**, 205701 (2015).
[402] R. Brendel and R. Peibst, IEEE J. Photovolt. **6**, 1413–1420 (2016).
[403] D. L. Young, W. Nemeth, V. LaSalvia, R. Reedy, S. Essig, N. Bateman, and P. Stradins, IEEE J. Photovolt. **6**, 41–47 (2016).
[404] D. L. Young, W. Nemeth, S. Grover, A. Norman, H.-C. Yuan, B. G. Lee, V. LaSalvia, and P. Stradins, Carrier selective, passivated contacts for high efficiency silicon solar cells based on transparent conducting oxides, in: Photovolt. Spec. Conf. (PVSC), 2014 IEEE 40th, IEEE, 2014: pp. 1–5. http://ieeexplore.ieee.org/document/6925147/ (accessed March 1, 2017).
[405] B. E. Deal, M. Sklar, a. S. Grove, and E. H. Snow, J. Electrochem. Soc. **114**, 266 (1967).
[406] T.-T. Li and A. Cuevas, Phys. Status Solidi RRL **3**, 160–162 (2009).
[407] X. Zhang and A. Cuevas, Phys. Status Solidi RRL **7**, 619–622 (2013).
[408] X. Zhang, S. Hargreaves, Y. Wan, and A. Cuevas, Phys. Status Solidi RRL **8**, 231–234 (2014).

